npj | robotics

Review

https://doi.org/10.1038/s44182-025-00040-5

Thin-film actuators (TFAs): a review

Zijing Zhang[1], Zhihua Liang[1] & Haimin Yao[1,2] ✉

Low-stiffness thin-film actuators (TFAs) have been attracting increasing attention in soft robotics, energy harvesting, and wearable technologies due to their programmable configurations, diverse deformation modes, and facile fabrication processes. This review summarizes recent progress in TFAs with a focus on their structural designs, fundamental mechanics, materials, and deformation mechanisms. Furthermore, we discuss their practical applications, challenges, and future opportunities, offering insights to guide the development of next-generation TFA innovations.

Actuators are indispensable devices applied in various engineering systems for exerting mechanical motions and forces, playing pivotal roles in automation, robotics, and agriculture, and enabling humans to handle complex and hazardous tasks that demand precise and controllable actuation[1]. Traditional actuators, such as relays, solenoids, and hydraulic cylinders, are known for their high energy efficiency, strong output force, and reliable power delivery (Fig. 1). However, their high rigidity, bulky structure, heavy weight, and inability to respond to ambient stimuli make them unsuitable for many emerging areas such as micro-robotics, wearable devices, and human-machine interfaces. To address these limitations, soft actuators with high compliance and flexibility were developed by using low-stiffness materials of a modulus of less than 1 GPa or slender structures that can undergo substantial deformation[2] (Fig. 1). The inherent softness of these actuators endows them with more degrees of freedom, high deformation controllability and tenderness of manipulation. Furthermore, the unique advantages of soft actuators, such as light weight, compactness, and high sensitivity to external stimuli, make them exceptionally suitable for executing intricate tasks such as minimally invasive surgery[3], assembling delicate components[4], and navigating in narrow space[5].

Soft actuators, based on their initial topologies before deformation, can be classified into three basic types: fiber type, thin-film type, and bulk type[6] (Fig. 1). Among them, thin-film actuators (TFAs) stand out for their programmability, integrability, and multi-functionality. A variety of responsive materials, such as carbon-based materials[7], liquid crystal polymers[8], shape memory alloys[9], and hydrogels[10], have been employed to produce TFAs via various manufacturing processes, including photolithography[11], coating[12], and deposition[13]. Upon external stimulations, TFAs morph into different morphologies through a variety of in-plane and out-of-plane deformation modes such as expansion/contraction, bending, twisting, or their combinations. Functional actions and locomotion, such as grabbing, crawling, and rolling, can be achieved by leveraging origami[14], tensegrity[15], and structural bistability[16], actuating soft robotics such as deployable crawlers[17], undulating swimmers[18], and snap-through-based jumpers[16]. Additionally, the planar structure of TFAs in combination with their adaptable fabrication processes makes it easy to integrate them with other accessory materials (e.g., conductive and adhesive materials) or peripheral components (e.g., electrical circuits). This paves the way for the development of all-in-one actuators that combine actuation, sensing, and energy harvesting together, advancing the development of energy harvesting systems and wearable devices[19].

Despite the remarkable potential of TFAs and significant progress in this vibrant field recently, the industrial applications of TFAs remain at a primary stage. In order to facilitate the transition of TFAs from laboratory prototypes to real-life products, it is essential to understand their fundamental working mechanisms, the latest research progress, and bottlenecking challenges faced for further development. In this review, we discuss the advancements in TFAs by presenting the up-to-date progress in this field (Fig. 2). First, we introduce the fundamental mechanics accounting for the basic bending deformation of TFAs, followed by an introduction to the responsive materials and fabrication processes for TFAs. Next, we overview the deformation mechanisms of TFAs with a highlight of their advantages and limitations. Subsequently, we showcase the representative applications of TFAs in emerging fields including biomimetic soft robotics, energy harvesting systems, and smart wearable devices. Finally, the review article is concluded by discussing the encountered challenges and outlooking the future opportunities and potential breakthroughs in the field of TFAs.

Basic Structures And Fundamental Mechanics

Most TFAs are bilayer structures consisting of an active layer and an inert layer. Upon stimulation, the active layer undergoes a significant in-plane deformation (either expansion or contraction), while the inert layer is relatively less responsive to the stimulus, resulting in a mismatch strain that drives an out-of-plane bending deformation of the whole structure. Generally, they are manufactured through depositions (PVD or CVD)[20], spin-coating[21], and electro-spraying[22]. The robustness of the interface between active and inert layers plays an important role in determining the durability of TFAs. To achieve high durability, TFAs with monolayer structure should be adopted, whose out-of-plane deformation relies on the in-plane strain with variation along the thickness direction[23]. Such inhomogeneous in-plane strain can be obtained by introducing either material heterogeneity[24] or gradient stimulation along the thickness direction[25]. To achieve response to multiple stimuli, TFAs with multilayer (>2 layers) were developed by integrating layers independently responsive to a specific stimulus[26].

[1]Department of Mechanical Engineering, The Hong Kong Polytechnic University, Hung Hom, Kowloon, Hong Kong SAR, China. [2]Research Center for Nature-inspired Science and Engineering, The Hong Kong Polytechnic University, Hong Kong, Hong Kong SAR, China. ✉e-mail: mmhyao@polyu.edu.hk

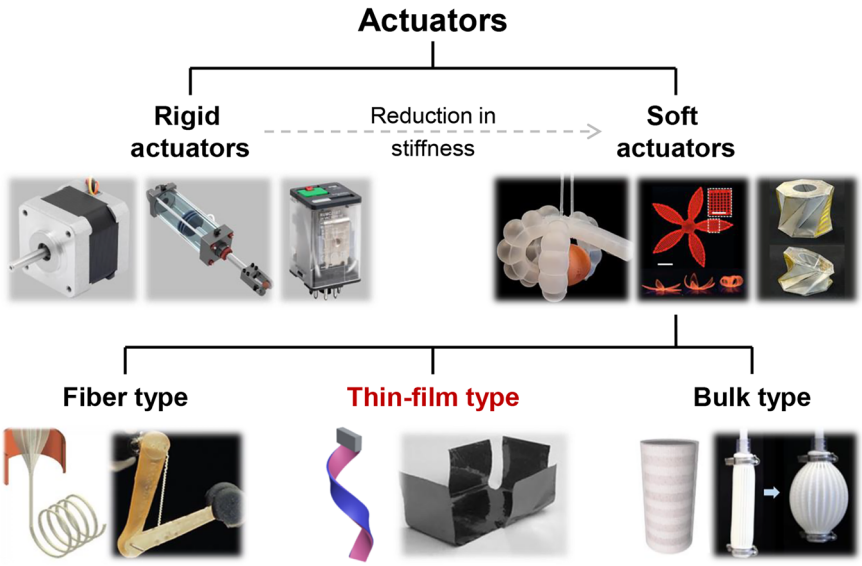

Fig. 1 | Classification of actuators. Based on their holistic stiffness, actuators can be roughly classified into rigid actuators and soft actuators, while soft actuators can be further categorized into fiber, thin-film, and bulk types according to their initial topologies.

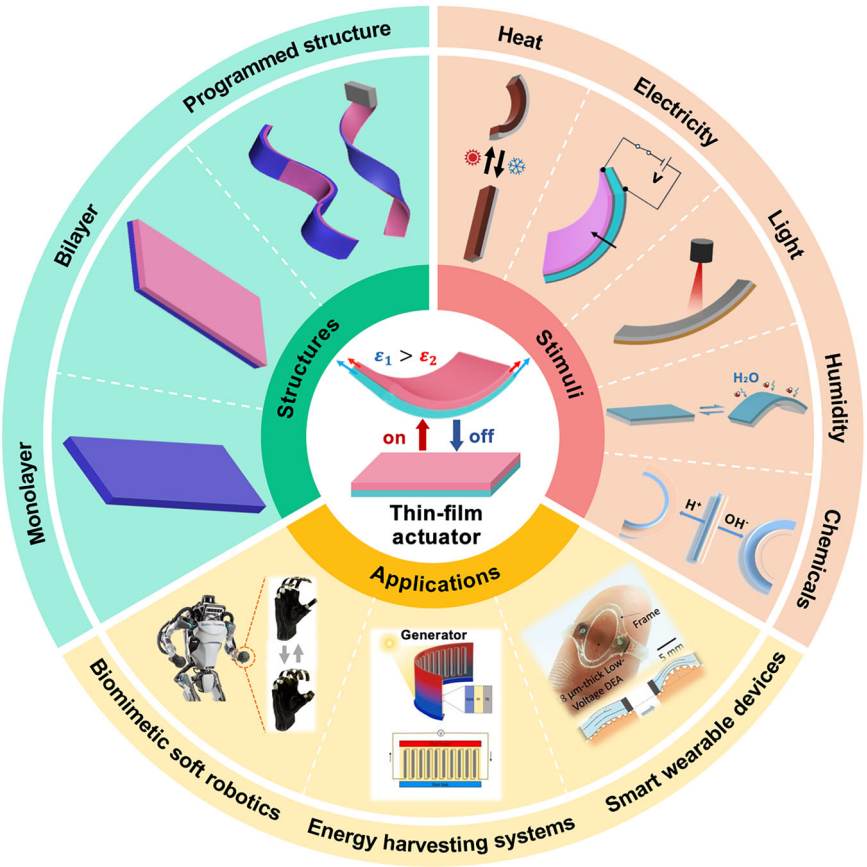

Fig. 2 | Overview of thin-film actuators (TFAs) in terms of their structures, stimuli, and applications. Reprinted with permission from ref. 115. Copyright 2024 MDPI. Reprinted with permission from ref. 116. Copyright 2021 Springer Nature. Reprinted with permission from ref. 117. Copyright 2023 Wiley-VCH. Reprinted with permission from ref. 118. Copyright 2015 Springer Nature. Reprinted with permission from ref. 47. Copyright 2020 American Chemical Society. Reprinted with permission from ref. 110. Copyright 2020 Wiley-VCH. Reprinted with permission from ref. 119. Copyright 2022 MDPI. Reprinted with permission from ref. 102. Copyright 2023 Wiley-VCH.

Although multilayer TFAs exhibit more sophisticated deformation modes and extended functions, they contain more heterogeneous interfaces and therefore suffer from the interfacial delamination problem. This limitation plus their complex fabrication processes, and lower controllability limit the wide application of multilayer TFAs.

Although the deformation mode of TFAs can be complicated through topological designs, the most basic deformation mode of TFAs is still bending. Understanding the fundamental mechanics accounting for the bending deformation of TFAs is of great importance to their design and control. Take the common bilayer-type TFA as an example. It can be simply modeled as an Euler-Bernoulli beam (plane stress assumption) consisting of an inert layer and an active layer (Fig. 3a). For simplicity of analysis, it is assumed that the active layer is much thinner than the inert layer ($h_{ac} \ll h_{in}$). Upon external stimulus, two layers expand differently, leading to a mismatch stain denoted by $\varepsilon_{mis} = \varepsilon^s_{in} - \varepsilon^s_{ac}$, where ε^s_{in} and ε^s_{ac} stand for the stimulus-induced strains of the inert layer and active layer respectively. For instance, the mismatch strain caused by temperature change $\triangle T$ is given by $\varepsilon_{mis} = (\alpha_{in} - \alpha_{ac})\triangle T$, where α_{ac}, α_{in} are the coefficients of thermal

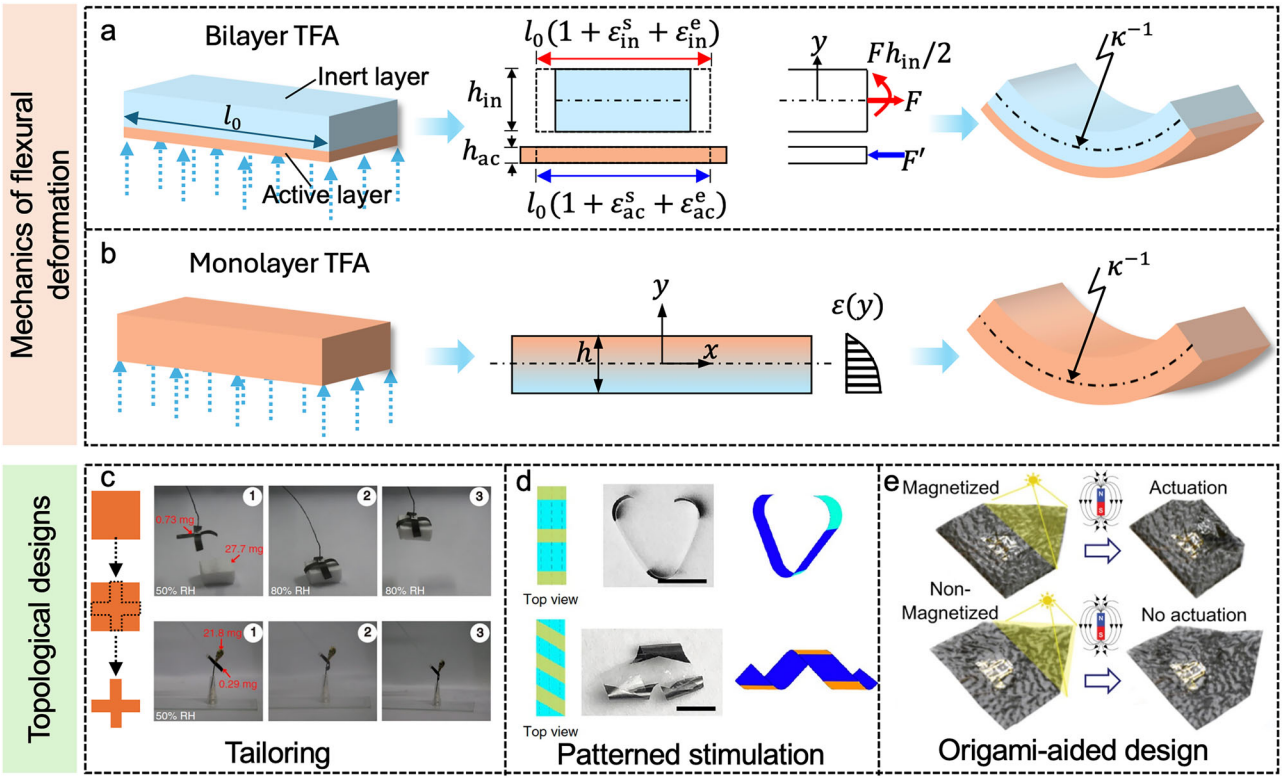

Fig. 3 | Schematic illustration showing the mechanics of flexural deformation and topological designs of TFAs. Reprint with permission from ref. 28. Copyright 2022 American Chemical Society. Reprint with permission from ref. 30. Copyright 2024 Wiley-VCH. Reprint with permission from ref. 31. Copyright 2021 Wiley-VCH.

expansion of the active and inert layers, respectively. To accommodate such mismatch strain across the heterogeneous interface, non-uniform but self-balanced stress must occur over the cross-section, resulting in flexural deformation of the TFA. The bending curvature κ, according to the Stoney relation for thin-film and substrate systems[27], can be written as

$$\kappa = \frac{6\sigma_{ac}h_{ac}}{E_{in}h_{in}^2} \tag{1}$$

where E_{in} is the plane-strain modulus of the inert layer and σ_{ac} is the mean stress in the active layer. Accommodation of the mismatch strain between two layers across the interface requires

$$\varepsilon^e_{ac} - \varepsilon^e_{in} = \varepsilon_{mis}$$

where $\varepsilon^e_{in}, \varepsilon^e_{ac}$ stand for the elastic strains of the inert and active layers close to the interface. Mechanics analysis based on the Euler-Bernoulli beam theory implies that $\varepsilon^e_{ac} = \frac{\sigma_{ac}}{E_{ac}}$ and $\varepsilon^e_{in} = -\frac{4\sigma_{ac}h_{ac}}{E_{in}h_{in}}$. From the above equations, the mismatch strain can be correlated with the mean stress in the active layer through

$$\varepsilon_{mis} = \left[\frac{1}{E_{in}} \bullet \frac{4h_{ac}}{h_{in}} + \frac{1}{E_{ac}}\right]\sigma_{ac} \tag{2}$$

Combining Eq. (1) and Eq. (2) to eliminate σ_{ac} yields the bending curvature as a function of the mismatch strain

$$\kappa = \frac{6h_{ac}}{h_{in}}\left[\frac{E_{ac}}{4E_{ac}h_{ac} + h_{in}E_{in}}\right]\varepsilon_{mis} \tag{3}$$

Equation (3) shows the proportionality between the bending curvature (κ) and the mismatch strain (ε_{mis}). This proportionality also applies to bilayer FTAs with the active layer and the inert layer of comparable thicknesses[27].

For a monolayer TFA (Fig. 3b) with homogenous properties (Young's modulus E, Poisson's ratio ν, and coefficient of stimulus-induced expansion α), basic mechanics analysis based on the Euler-Bernoulli beam model (plane stress assumption) indicates that the axial stress caused by a non-uniform stimulation $\triangle S(y)$ is given by

$$\sigma_x(y) = -E\varepsilon^s(y) + \frac{E}{h}\int_{-h/2}^{h/2}\varepsilon^s(y)dy + \frac{12yE}{h^3}\int_{-h/2}^{h/2}\varepsilon^s(y)ydy$$

where h is the thickness of the TFA and $\varepsilon^s(y) = \alpha\triangle S(y)$. The variation of stimulation along the longitudinal direction (x-direction) is neglected. It can be verified that $\sigma_x(y)$ is self-balanced as $\int_{-h/2}^{h/2}\sigma_x(y)dy = 0$ and $\int_{-h/2}^{h/2}y\sigma_x(y)dy = 0$. The elastic strain induced by this self-balanced stress is given by

$$\varepsilon^e(y) = \frac{\sigma_x(y)}{E} = -\varepsilon^s(y) + \frac{1}{h}\int_{-h/2}^{h/2}\varepsilon^s(y)dy + \frac{12y}{h^3}\int_{-h/2}^{h/2}\varepsilon^s(y)ydy$$

The total strain (ε^t), which is equal to the summation of the elastic strain and the stimulus-induced strain, is given by

$$\varepsilon^t(y) = \varepsilon^e(y) + \varepsilon^s(y) = \frac{1}{h}\int_{-h/2}^{h/2}\varepsilon^s(y)dy + \frac{12y}{h^3}\int_{-h/2}^{h/2}\varepsilon^s(y)ydy$$

The first term on the righthand side of the above expression is independent of y and therefore leads to no bending deformation, while the second term is a linear function of y, which leads to a flexural configuration

Table 1 | Comparison of responsive materials applied in TFAs

TFA type	Responsive materials	Favorable material properties	Fabrication processes
Thermo-driven	• PDMS • Shape memory alloys • Graphene • MXene	• High thermal stability • High flexibility • High ductility • High thermal expansion coefficient	• Casting • Molding • Direct bonding • PVD/CVD
Electro-driven	• Conductive carbon materials • Dielectric elastomers • Ionic polymer-metal composites	• High electrical conductivity • High dielectric constant • High thermal stability • Fast response	• Lamination • Electrospinning • Casting • Molding
Light-driven	• Graphene • Carbon nanotubes (CNTs) • Liquid crystal elastomers (LCEs) • Azobenzene-based polymer	• High photothermal conversion efficiency • Photo-reactivity • Wavelength selectivity • High light transmittance	• Vacuum filtration • Casting • Coating • Self-assembly
Humidity-driven	• Graphene oxide • Carbon nanotubes (CNTs) • MXene • Cellulose • Sodium alginate	• High hygroscopic stability • High flexibility • High hygroscopic expansion coefficient • Water diffusivity	• Vacuum filtration • Hot pressing • Chemical cross-linking
Chemical-driven	• Polyacrylate • Polyamino acids • PVDF	• High pH or chemical vapor sensitivity • Reversibility • High chemical stability	• Casting • Electrospinning • Chemical cross-linking

with curvature κ given by

$$\kappa = \frac{12}{h^3}\int_{-h/2}^{h/2} \varepsilon^s(y) y dy \quad (4)$$

Equation (4) shows the dependence of the bending curvature (κ) of monolayer TFAs on the distribution of stimulus-induced strain $\varepsilon^s(y)$. If $\varepsilon^s(y)$ is constant, which implies a uniform distribution of the stimulus-induced strain along the thickness direction, no bending deformation would be produced. Furthermore, if $\varepsilon^s(y)$ is an even function of y, no bending deformation would happen either, implying that an asymmetric stimulus-induced strain is crucial for inducing bending deformation in monolayer TFAs.

Although TFAs with simple rectangular or circular shapes merely exhibit bending deformation upon stimulation, more complex and controllable morphologies can be acquired if prior topologies are introduced[28] (Fig. 3c). For example, a humidity-driven TFA was tailored into biomimetic shapes to achieve curling and grabbing[26]. Another strategy for realizing complex morphologies is to distribute the active layer or materials in a designed pattern through partial oxidation[23], local thickness modification[29], or partial doping[30] (Fig. 3d). More complex 3D morphologies can be achieved by leveraging origami-inspired strategies such as pre-designed folding patterns or programmed creases into TFAs[31] (Fig. 3e). In our above discussion on deformation mechanics of thin-film actuators (TFAs), we have not distinguished the material base of the stimulus-induced strains, which will be elaborated in the following section.

Responsive Materials For Tfas

Based on the stimuli that active materials respond to, TFAs can be basically divided into five categories, including thermo-driven, electro-driven, light-driven, humidity-driven, and chemical-driven TFAs. Table 1 summarizes the typical responsive materials, favorable material properties, and fabrication processes of each type of TFAs.

Thermo-driven TFAs demand responsive materials with high coefficient of thermal expansion and high thermal stability as well as mechanical flexibility and ductility. Materials like shape memory alloys (SMAs)[32,33], polydimethylsiloxane (PDMS)[34], polyethylene (PE)[35], liquid crystal elastomers (LCEs)[36], graphene[29], and MXene[37] have been widely applied to fabricate thermo-driven TFAs with methods of casting, molding, directing bonding, and physical or chemical vapor deposition (PVD/CVD)[38].

Electro-driven TFAs call for responsive materials with enhanced electrothermal effect, high conductivity, high dielectric strength, and high thermal stability. Dielectric elastomers[39], conductive carbon materials[40,41], and ionic polymers[42] are often applied to fabricate electro-driven TFAs for their high electrical responsiveness and significant deformability. The fabrication techniques of electro-driven TFAs include lamination, electrospinning, direct casting, and molding.

Light-driven TFAs rely on responsive materials with superior optical properties for achieving specific functions, including high photothermal conversion efficiency for thermo-induced volume change, strong photo-reactivity for effective light absorption, wavelength selectivity for controllable responses, and high light transmittance for enhanced illuminance on the active material. Graphene[43], carbon nanotubes (CNTs)[43], LCEs[36], and azobenzene-based polymers[44], which possess foregoing desirable characteristics, are regarded as ideal candidates for light-driven TFAs. Common fabrication techniques of light-driven TFAs include vacuum filtration, spin coating, casting, and self-assembly.

Humidity-driven TFAs rely on the swelling behavior of hygroscopic materials. In addition to a high hygroscopic swelling coefficient, an ideal responsive material for humidity-driven TFAs should also possess high flexibility, appropriate water diffusivity, and high hygroscopic stability. Prevailing responsive materials for humidity-driven TFAs include cellulose, sodium alginate (SA), graphene oxide (GO), CNTs[45,46], and MXene[37]. These materials absorb water molecules, resulting in an inhomogeneous strain that causes bending or swinging motions. Hot pressing, chemical cross-linking, and vacuum filtration are manufacturing methods often adopted to fabricate these actuators.

Chemical-driven TFAs rely on materials responsive to pH change or specific chemical vapors such as polyaniline[47], polyacrylic acids[47], and PVDF[48]. Casting, electrospinning, and chemical cross-linking are techniques frequently used to produce thin, uniform films with these materials, resulting in reversible expansion or bending behaviors in response to specific chemical stimuli.

Understanding these stimulus-responsive materials offers a foundation for the design of TFAs for specific environmental or operational needs. With this, we further delve into the deformation mechanisms of TFAs to obtain insights into how external stimuli trigger the mechanical motion and morphing of TFAs.

Deformation Mechanisms Of Tfas

The deformation mechanisms of TFAs refer to the physical or chemical processes that generate stimulus-induced strain in the active materials. Understanding the deformation mechanisms of TFAs is crucial for selecting appropriate application scenarios and addressing limitations for further advancements of TFAs.

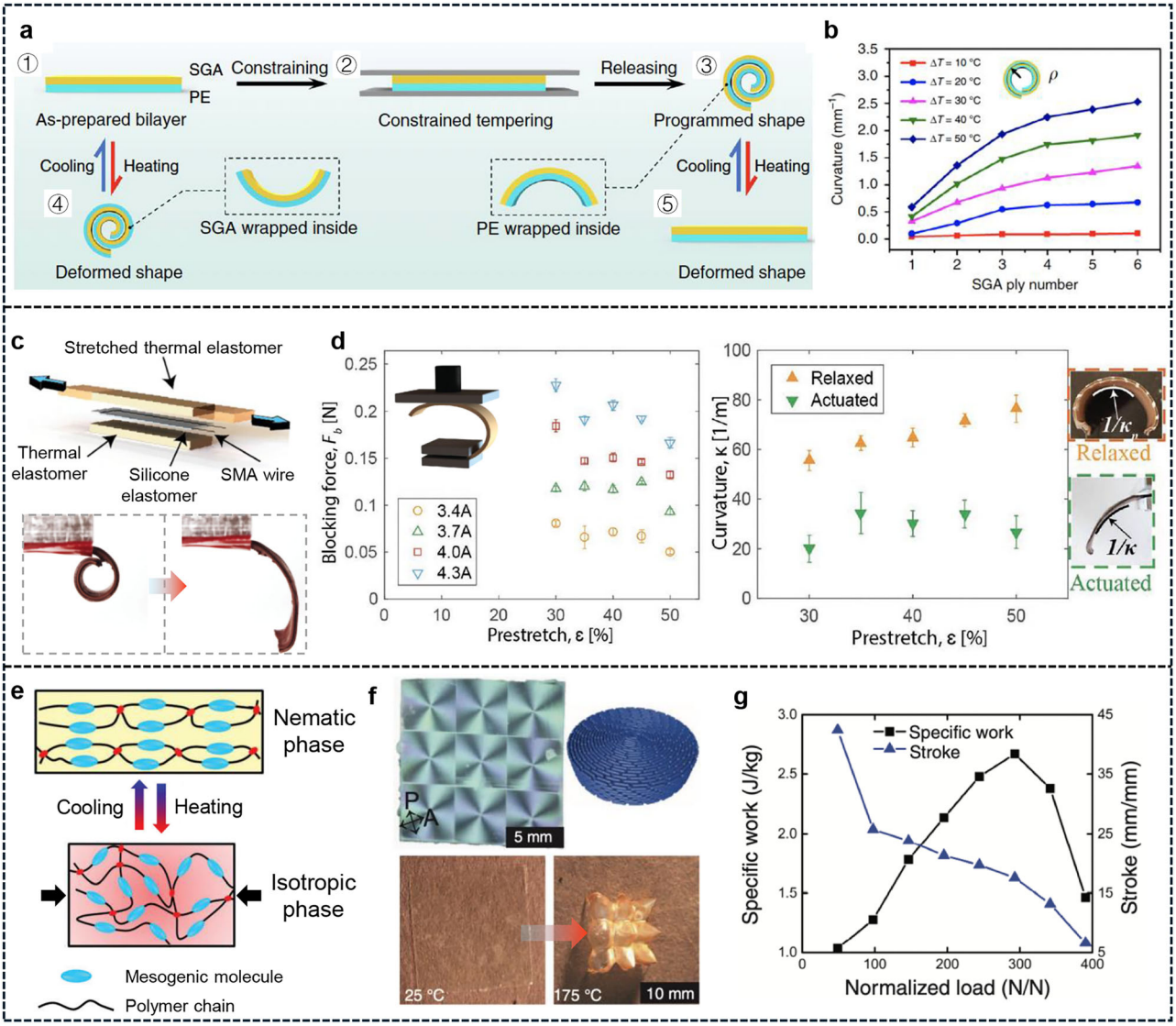

Fig. 4 | Typical TdTFAs. a SGA-based TdTFAs and the constrained tempering process. **b** Bending curvature of SGA-based TdTFAs with different ply numbers. **c** The multilayer structure of SMA-based TdTFAs. **d** Blocking force and bending curvature generated by the SMA-based TdTFAs. **e** Deformation mechanism of LCEs. **f** LCE-based TdTFA transforms from flat to corrugated upon heating. **g** Specific work and stroke produced by LCE-based TdTFAS. **a**, **b** Reprinted with permission from ref. 45. Copyright 2020 Springer Nature. **c**, **d** Reprinted with permission from ref. 50. Copyright 2019 Wiley-VCH. **e** Reprinted with permission from ref. 36. Copyright 2018 Royal Society of Chemistry. **f**, **g** Reprinted with permission from ref. 51. Copyright 2019 American Association for the Advancement of Science.

Deformation mechanisms of thermo-driven thin-film actuators (TdTFAs)

TdTFAs convert thermal energy into mechanical deformation by leveraging the thermal-induced volume change of materials[45], which occurs due to the increase of equilibrium distance between atoms upon heating or thermo-induced phase transformation/transition. For bilayer TdTFAs, the different thermal expansion properties between the active and inert layers induce strain mismatch and therefore bending deformation. For monolayer TdTFAs, the bending deformation results from the strain gradient within the film.

The most widely used deformation mechanism in TdTFAs relies on the expansion of atomic spacing due to heating. Materials including polymer (PE, PC) and 2D materials (MXene, GO) have shown great promise[45,49]. To enhance the programmability of these TdTFAs, Wang et al. developed programmable TdTFAs using stacked graphene assembly (SGA) as the inert layer and PE as the active layer[45] (Fig. 4a, b). The resulting SGA/PE bilayer film exhibited sensitive morphing behaviors in response to the variation of the surrounding temperature. More interestingly, the initial configuration of such TdTFA was programmed by leveraging a constrained tempering process. This is basically attributed to the asymmetric elastoplasticity of the SGA—elastic under compression and plastic under tension. Meanwhile, to achieve complex morphologies, the initial topologies of this TdTFA were customized by patterning the active material or localized heating, making it capable of twisting, curling, and locomotion upon heating.

Another deformation mechanism of TdTFAs is thermo-induced phase transformation/transition, which alters material properties such as rigidity, density, and strength. For example, SMAs are a group of alloys that exhibit a reversible change in both shape and rigidity owing to the phase transformation between the monoclinic martensite (low temperature) and cubic austenite phases (high temperature). At low temperatures, SMA is in the martensite phase and can be easily formed due to its monoclinic structure and lower rigidity. When heated, the phase transformation from the martensite phase to the austenite phase occurs, leading to the release of the residual stress and recovery of the original shape[32]. Based on this mechanism, Huang et al. developed a TdTFA with a SMA layer sandwiched between two thermally conductive elastomer layers[50] (Fig. 4c). One elastomer layer is pre-stretched before bonding with the other layers, resulting in a curled initial configuration of the TdTFA. Upon heating above the phase transition

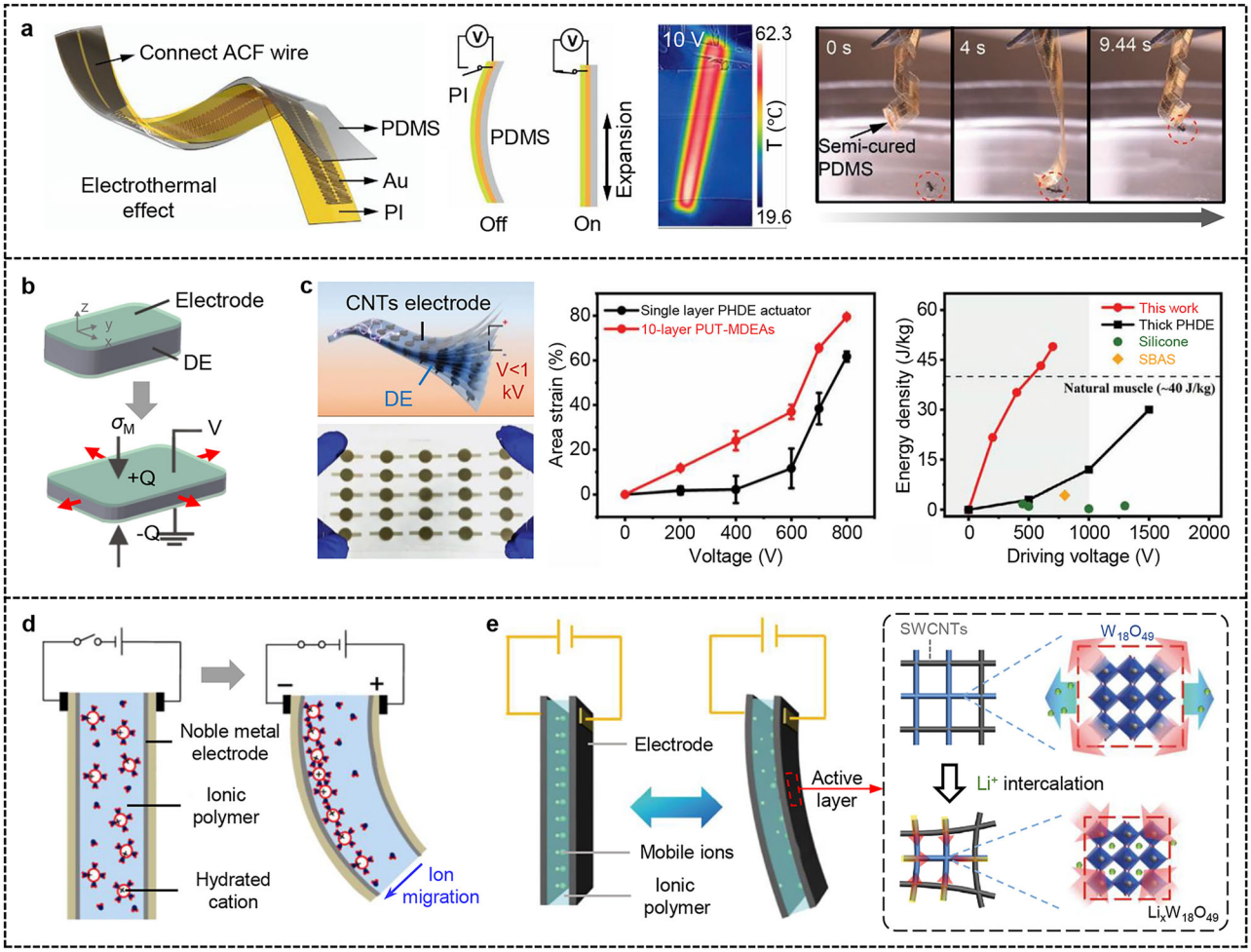

Fig. 5 | Typical EdTFAs. a Deformation mechanism of an electrothermal EdTFA composed of PDMS as the active layer, polyimide as the inert layer, and a gold electrode as the heating element. **b** Deformation mechanism and the structure of a DE-based EdTFA. **c** Multilayer DE-based EdTFAs with low driving voltage and high performance. **d** Deformation mechanism and the structure of an IP-based EdTFA with inert electrodes. **e** Deformation mechanism and the structure of an IP-based EdTFA with active electrodes and the structural evolution of W18O49 lattice owing to the Li+ intercalation. **a** Reprinted with permission from ref. 52. Copyright 2021 Wiley-VCH. **b** Reprinted with permission from ref. 39. Copyright 2022 IOP Publishing. **c** Reprinted with permission from ref. 40. Copyright 2024 Wiley-VCH. **d** Reprinted with permission from ref. 42. Copyright 2014 American Chemical Society. **e** Reprinted with permission from ref. 64. Copyright 2018 Springer Nature.

temperature, the shape memory effect of the SMA layer is triggered, leading to the unfolding of the coiled actuator and storage of elastic energy in the elastomer layers. After cooling, the TdTFA recovers to its curled configuration due to the phase transformation from austenite to martensite phase and the relaxed elastic energy in the elastomers (Fig. 4d).

In addition to SMAs, thermo-responsive polymers (e.g., LCEs) also achieve actuation through thermo-induced phase transition. In the initial state of LCE, the rod-like mesogenic molecules within these polymers exhibit preferential alignment. Once heated above the phase transition temperature, a nematic-to-isotropic phase transition occurs and the mesogenic molecules become randomly aligned[8,36] (Fig. 4e), resulting in the deformation of the LCE. The LCE-based TdTFAs can be engineered with designed molecular alignment and thus the controllable morphologies[51] (Fig. 4f, g). Compared to SMA-based TdTFAs, LCE-based TdTFAs display lower stiffness, larger deformation, faster response time, and lower activation energy, making them more attractive in biomedical devices and wearable technology.

Despite significant advancement in TdTFAs, technical barriers to their wide applications remain. Firstly, the thermal stimuli of TdTFAs may accelerate the degradation of the active materials, especially the organic and polymeric ones. Another limitation is their low response speed, which can be attributed to the tardiness of heat transfer processes. Besides, the conversion of thermal energy into mechanical energy is inherently inefficient, leading to significant energy loss.

Deformation mechanisms of electro-driven thin-film actuators (EdTFAs)

The primary deformation mechanism of EdTFAs is thermal expansion caused by Joule heating of the electrical current passing through conductive materials. The different thermal expansions between layers result in a mismatch strain upon Joule heating, leading to bending or coiling deformation of the actuators. Typical conductive materials used for Joule heating include metallic films[52], CNTs[53], graphene[54], and MXene[55]. These materials can be either coated onto or doped into a film with a high thermal expansion coefficient (e.g., PDMS and PE). In multilayer EdTFAs, a separate conductive layer is adopted for Joule heating. For instance, Li et al. developed a three-layer EdTFA, which is composed of an active layer (PDMS), an inert layer (polyimide), and a serpentine gold layer for heating[52] (Fig. 5a). These EdTFAs exhibit remarkable flexibility and rapid response rates, enabling them to capture insects via coiling.

Another deformation mechanism of EdTFAs is contraction induced by electrostatic pressure, which often takes place in dielectric elastomers (DEs) subjected to high voltage. A typical DE-based EdTFA consists of a DE film sandwiched between two compliant electrodes[56]. When a voltage is applied, the electrostatic pressure arising from Coulomb forces between the oppositely charged electrodes acts on the elastomer, causing contraction along the thickness direction and expansion along the in-plane directions[57] (Fig. 5b). For better actuation performance, DE materials with low elastic

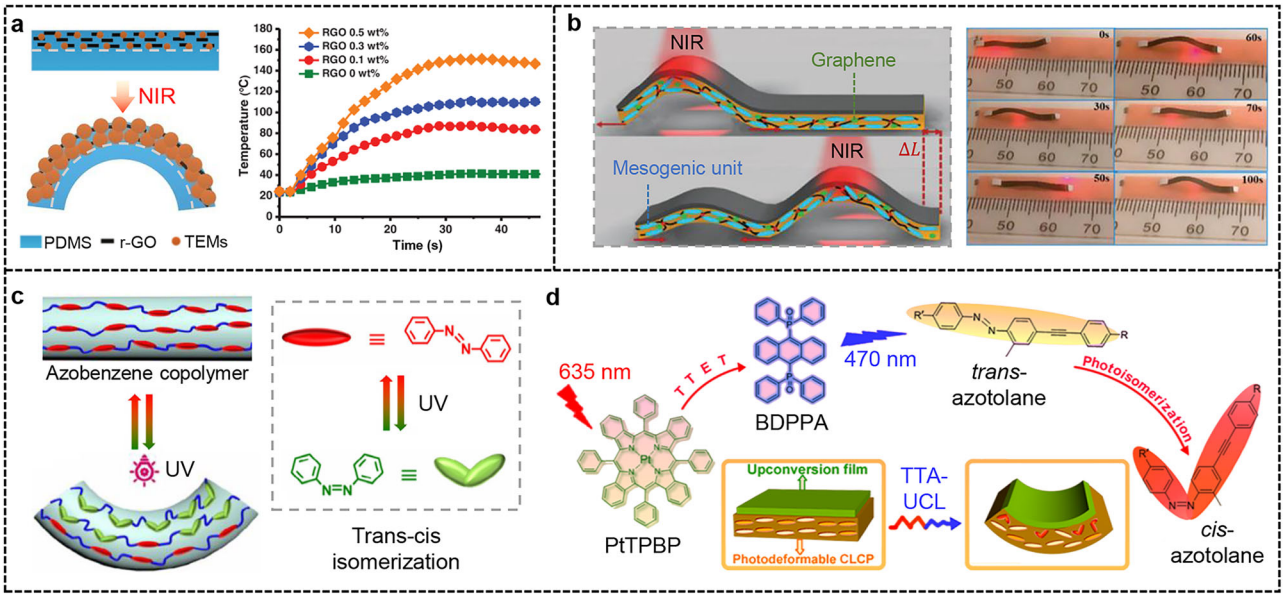

Fig. 6 | Typical LdTFAs. a Deformation mechanism of photothermal bilayer LdTFAs based on the expansion of TEMs and the temperature evolutions of LdTFAs for different r-GO concentrations. **b** Deformation mechanism of photothermal LdTFAs based on LCE phase transition. Directional crawling of a LdTFA-based artificial worm driven by controlled NIR irradiation. **c** Deformation mechanism of azobenzene-based LdTFAs and the trans-cis isomerization of azobenzene under UV irradiation. **d** Working principle of red-light-controlled LdTFAs based on a red-to-blue TTA-based conversion system. **a** Reprinted with permission from ref. 43. Copyright 2017 Wiley-VCH. **b** Reprinted with permission from ref. 36. Copyright 2018 Royal Society of Chemistry. **c** Reprinted with permission from ref. 44. Copyright 2024 American Chemical Society. **d** Reprinted with permission from ref. 76. Copyright 2013 American Chemical Society.

modulus, high breakdown strength, and high dielectric constant are preferred, such as acrylic elastomers[58] and polyurethane[59]. Materials with high conductivity, high flexibility, and good conformability with DEs, including graphene[56], CNTs[56], and conductive polymers[57], are commonly applied as electrodes of EdTFAs. However, the high driving voltage (typically several kilovolts) required by DE films remains a bottleneck problem limiting their wider applications. To reduce the driving voltage, new materials and structural designs are adopted. For example, a high-performance DE-based EdTFA capable of operating at hundreds of volts was developed by employing a multilayer ultra-thin DE film, achieving significant areal strain (80%) and considerable output pressure (0.16 MPa) and energy density (50 J/kg)[40] (Fig. 5c).

The third deformation mechanism of EdTFAs relies on the volume change of active materials induced by ion migration or ion intercalation/deintercalation. Typically, these EdTFAs feature a three-layer structure, where an ionic polymer (IP), such as Nafion[60] and PVDF[61], is sandwiched between two electrodes. These IPs contain ionizable functional groups and mobile ions, enabling them to conduct ions when hydrated or solvated[62]. When an electric field is applied through two electrodes, hydrated cations (e.g., $Na^+(H_2O)_n$) migrate toward the cathode. This directional ion migration causes local expansion of the IP near the cathode, resulting in bending of the EdTFAs toward the anode[60] (Fig. 5d). If intercalation host materials (e.g., $W_{18}O_{49}$ or V_2O_5) are adopted as electrodes, volume change of the electrodes would take place due to ion intercalation and deintercalation driven by electric field[63], which could also be applied to drive the EdTFAs. For example, a $W_{18}O_{49}$ NWs/SWCNTs composite lattice was applied as electrodes of an IP-based EdTFA (Fig. 5e). Upon voltage application, active ions (e.g., Li^+) in the IPs move toward the cathode and intercalate into the electrode layers. This intercalation triggers a phase transition of $W_{18}O_{49}$ NWs, forming $Li_xW_{18}O_{49}$ through the faradaic redox reaction ($W_{18}O_{49} + xLi^+ + xe^- \leftrightarrow Li_xW_{18}O_{49}$), accompanied by lattice contraction[64] (Fig. 5e). The resulting volume reduction generates a mismatch strain between the anode and cathode layers, causing the EdTFAs to bend toward the cathode.

The actuation characteristics of EdTFAs such as frequency and amplitude can be precisely controlled by modulating the applied electrical current, waveform, and voltage. Such exceptional controllability, in combination with rapid response rate and high precision, makes them applicable in microelectromechanical systems, wearable devices, and soft robotics. However, the wide application of EdTFAs encounters some practical challenges, including complex power supply requirements, heat generation during prolonged operation, and material compatibility issues.

Deformation mechanisms of light-driven thin-film actuators (LdTFAs)

Most LdTFAs are driven by the photothermal effect which can be observed from many photothermal materials such as carbon-based materials[65], MXene[66], metal nanoparticles[67], and organic molecular dyes[68]. Normally, photothermal materials are integrated with thermo-responsive materials to form active layers of bilayer LdTFAs. When absorbing light in a specific wavelength range, the photothermal phase in the active layer converts the light energy into thermal energy, which induces expansion or phase transitions of the thermo-responsive phase, resulting in a volume change of the active layer[69]. For example, Tang et al. fabricated the active layer of a bilayer LdTFA by dispersing r-GO and thermally expanding microspheres into PDMS[43]. Under near-infrared (NIR) irradiation, the r-GO causes a rapid temperature increase from 20 °C to 110 °C, which triggers significant volume expansion of the microspheres and the active layer (Fig. 6a). Dong et al. developed a bilayer LdTFA by doping a LCE layer with graphene and pairing it with an inert layer made of acrylic ester[36], The contraction of LCE under NIR irradiation makes the actuator bend toward the active layer side. The resulting LdTFA exhibits high flexibility, rapid response, and spatially localized response, enabling it to mimic the crawling motion of a worm under controlled NIR irradiation (Fig. 6b).

In addition to the photothermal effect, the photochemical effect, which is exhibited by photo-responsive molecules such as azobenzene[70], spiropyran[71], and diarylethenes[72], is also often applied in LdTFAs. In practice, these photo-responsive molecules are commonly incorporated with soft matrices such as elastomers, liquid crystal materials, or hydrogels. The photochemical process of photo-responsive molecules induces changes in molecular geometry, including trans-cis isomerization, ring opening and closing, cycloadditions, and bond exchange[73]. For instance, under UV

irradiation, azobenzene undergoes a transition from a stable rod-like trans configuration to a bent cis configuration, leading to volume contraction of the elastomers or gels matrix due to altered molecular spatial requirements[74] (Fig. 6c). In azobenzene-doped LCE-based LdTFA, trans-cis isomerization also disrupts the alignment of liquid crystal molecules, resulting in significant contraction of the LCEs along the alignment direction[75]. However, conventional photochemical LdTFAs are typically driven by blue or UV light, which exhibits high phototoxicity and energy requirements, limiting their use in biomedical applications. To overcome this challenge, materials capable of converting wavelength have been applied in LdTFAs. This enables actuation control via red light, which offers deep penetration in biological tissues, minimal photodamage, and low energy requirements. A notable example is the red-light-controlled LdTFAs developed by Yu et al., which is composed of a wavelength-conversion film and azobenzene-doping liquid crystal polymer (LCP)[76]. The wavelength-conversion film absorbs the red light (635 nm) and emits the blue light (470 nm), which is absorbed by azobenzene molecules in the LCP, causing the bending of the actuator (Fig. 6d).

LdTFAs offer unique advantages in terms of wireless control and spatiotemporal precision, enabling applications in delicate or hazardous environments where direct physical contact ought to be avoided. However, their operation usually relies on an unimpeded light path, restricting their application in convoluted spaces like curved pipelines. Additionally, the performance of LdTFAs can be affected by light scattering in adverse environments, and the actuation efficiency depends strongly on the wavelength matching between the light sources and the responsive materials. Continuous research efforts should be made to improve photomechanical conversion efficiency and broaden the spectrum of stimulating light.

Deformation mechanism of humidity-driven thin-film actuators (HdTFAs)

HdTFAs utilize hygroscopic materials with abundant polar molecules or groups to absorb water molecules from the environment, resulting in volume expansion[77,78]. The primary deformation mechanism of HdTFAs is water-induced swelling of the concerned materials. For instance, stacked assembly of flakes of 2D materials like MXene and GO are commonly employed as hygroscopic materials in HdTFAs[78] due to the abundant water-attractive hydroxyl functional groups in them. The absorption of water molecules expands the d-spacing between the nanoflakes of the stacked assemblies, resulting in hygroscopic expansion. In 2020, Fan et al. applied MXene to develop a monolayer HdTFA[25] (Fig. 7a). The actuator, when placed above hot water (40°C), can flip back and forth. If clamped at one end, it will swing up and down automatically[25] (Fig. 7b). Similar flapping motion under steady humidity stimulation can also be achieved by GO-based HdTFAs (Fig. 7c, d)[23], implying the presence of a common governing mechanism which remains obscure so far.

Another deformation mechanism of HdTFAs is the breakage of chemical bonds in hygroscopic materials such as polyimide (PI)[79], and sodium alginate (SA)[30]. For instance, SA swells upon water absorption as water molecules penetrate its polymer network, disrupting intermolecular hydrogen bonds and turning the polymer chains into a hydrated structure. Meanwhile, SA is composed of β-D-mannuronic acid (M-blocks) and α-L-guluronic acid (G-blocks). These acid units contain abundant carboxyl groups. They can form hydrogen bonds and generate electrostatic interactions with water molecules, leading to further hygroscopic swelling. In 2023, Lu et al. applied SA as the active material and PDMS as the inert material to develop a bilayer HdTFA[30] (Fig. 7e, f). Upon water absorption, the active SA layer expands and causes the bending of the actuator. However, this mechanism suffers from a long recovery time due to the slow polymer chain relaxation during desorption and the poor mechanical properties due to the degradation of SA in humidity. To address these limitations, carbon nanofibers (CNF) as the enhancement are added into SA[80] (Fig. 7g, h). Meanwhile, the abundant hydroxyl groups in CNF endow the HdTFA with high humidity responsiveness. Furthermore, the higher specific area of CNF promotes water desorption, which facilitates the recovery of the HdTFAs in less-humid environments.

Despite these advancements of HdTFAs, several questions remain unsolved. First, the increase of d-spacing between the nanoflakes in 2D materials-based films may not lead to in-plane expansion, which is necessary for its bending deformation. However, it remains unclear what causes the in-plane expansion in these 2D materials-based films. Additionally, the autonomous flapping behavior of HdTFAs under steady stimulation implies a reversible water absorption and desorption mechanism coupled with the dynamic water transport across film thickness. Revealing this mechanism is crucial for better applications of HdTFAs in practice.

Deformation mechanisms of chemical-driven thin-film actuators (CdTFAs)

In addition to water, chemical substances, either in liquid or vapor state, can also be applied to actuate responsive materials. According to the chemical stimuli to respond, CdTFAs can be classified into pH-responsive type and organic solvent-responsive type.

pH-responsive CdTFAs are typically developed from ionizable polymers with pendant groups in their backbone that undergo ionization in response to pH changes, generating polyanions, polycations, and polyzwitterions[81]. The ionizable polymers can be classified into anionic polymers and cationic polymers based on their pH-dependent charging behavior[82]. Anionic polymers attract negative charges and form polyanions by deprotonation of their pendant groups (e.g., carboxyl groups) when the environmental pH is greater than their dissociation constant (pK_a) (Fig. 8a). Conversely, cationic polymers form polycations through protonation in acidic environments (Fig. 8a). The electrostatic repulsion between similar charges causes the polymer chains to expand. Meanwhile, the charged groups attract counterions from the solution, raising the internal osmotic pressure of polymers and driving water influx to equilibrate ion concentration. Together, these effects induce swelling of the polymer. For example, the bilayer pH-responsive CdTFAs, composed of anionic polymer (polyacrylic acid) and cationic polymer (polyacrylamide), achieves bidirectional bending through asymmetric swelling under gradually decreasing pH conditions (Fig. 8b). In addition, volume expansion resulting from polymer cleavage has also been applied to drive TFAs. Polymers containing acid-cleavable groups (e.g., hydrazine group) can undergo cleavage in an acidic environment, generating charged moieties and altering internal ionic concentration[83]. The pH fluctuations can modulate the degree of dissociation, disrupting hydrogen bonds between chains and reducing crosslinking density, ultimately causing volume expansion of polymers (Fig. 8c). Since the swelling of acid-cleavable polymers is typically irreversible, they are always designed for single-use scenarios like targeted drug release[84].

As the absorption of organic solvents by some polymers induces swelling, organic solvents are often applied as stimuli to drive the TFAs. Organic-solvent-responsive CdTFAs are engineered to selectively adsorb or interact with volatile organic solvents (liquid or vapor state), such as acetone[48] and ethanol[85]. This property makes them exceptionally valuable for applications requiring solvent detection or control. For example, poly(vinylidene fluoride) (PVDF) is particularly suitable for CdTFAs due to the substantial swelling induced by the transition from the β-PVDF phase to the α-PVDF phase after acetone absorption. When a PVDF film is exposed to an acetone vapor flow, the phase transition from β-phase to α-phase begins from one side to the other, resulting in an inhomogeneous distribution of the two phases and bending deformation of the film[48] (Fig. 8d, e). In addition to acetone, ethanol vapor is another chemical stimulus for CdTFAs. For example, Zhang et al. developed covalent organic framework (COF-42) membranes by using linear polymers as the building blocks, which will transfer to a swelling chiral phase when exposed to ethanol vapor. This solvent-responsive CdTFA shows a short response time (~1 s) and a significant bending curvature (~32 cm^{-1})[85].

CdTFAs exhibit distinct advantages, including high sensitivity to weak signals in the environment, stimuli specificity for targeted materials or conditions, and biocompatibility of their constituent materials, making

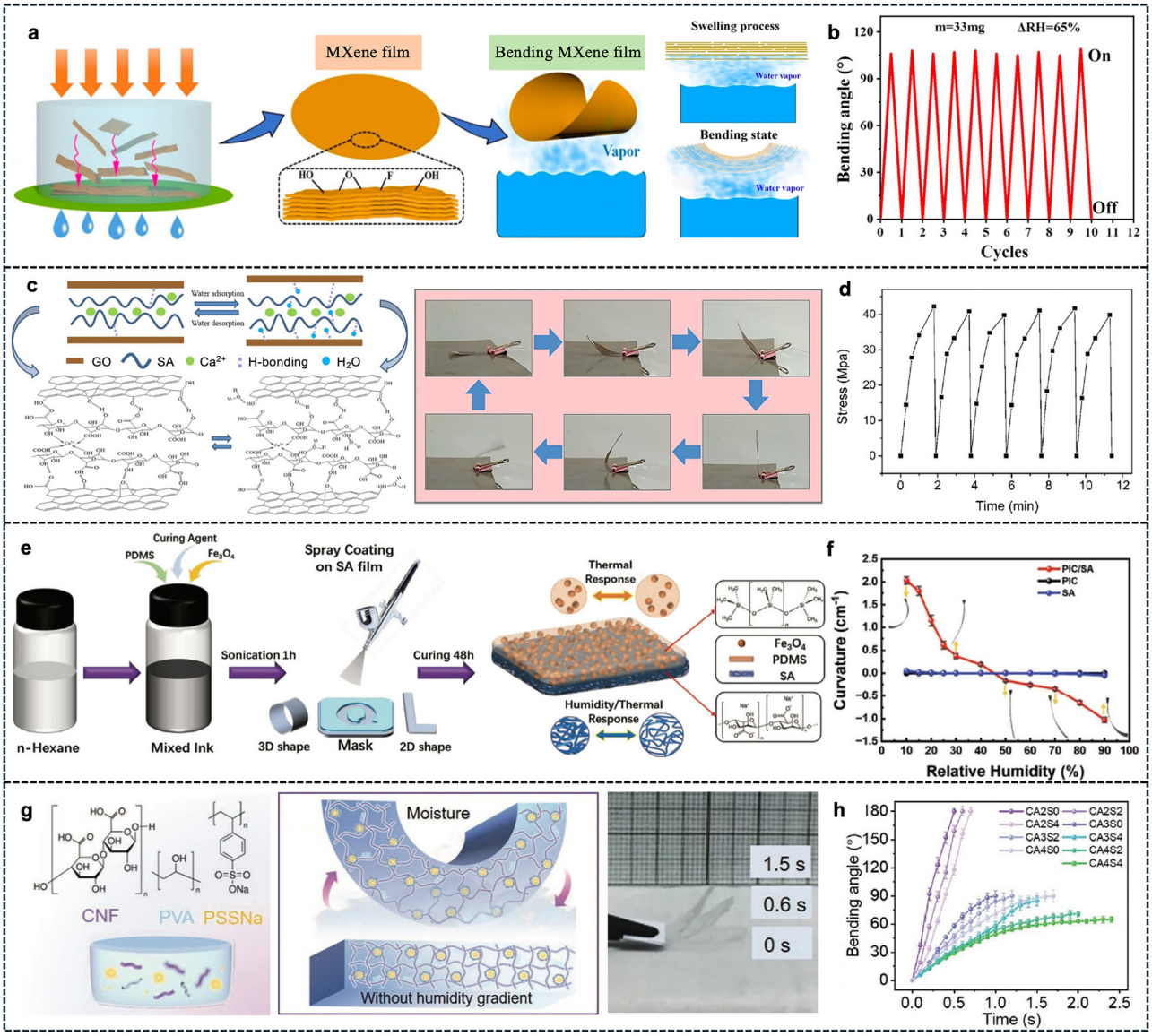

Fig. 7 | Typical HdTFAs. a Fabrication processes of MXene-based HdTFAs. **b** Swinging motions of MXene-based HdTFA in water vapor. **c** Deformation mechanism of GO/SA-based HdTFAs and its reciprocating response in gradient humidity field. **d** Stress variation of GO/SA film in humidity as a function of time. **e** Fabrication processes of TFA made by Fe3O4, PDMS and sodium alginate. **f** Response of PIC/SA, PIC, and SA to different humidities. **g** Deformation mechanism of CNF-, PVA- and PSSNa-based HdTFAs. **h** Bending angle response of CAS film upon humidity stimulation. **a**, **b** Reprinted with permission from ref. 25. Copyright 2020 Wiley-VCH. **c**, **d** Reprinted with permission from ref. 23. Copyright 2019 American Chemical Society. **e**, **f** Reprinted with permission from ref. 30. Copyright 2024 Wiley-VCH. **g**, **h** Reprinted with permission from ref. 80. Copyright 2022 Wiley-VCH.

them highly promising for biomedical and sensing applications. However, their widespread application is hindered by several critical limitations, such as slow response kinetics due to diffusion-limited mass transport, swelling/deswelling hysteresis during cyclic operation, and potential solvent toxicity.

Figure 9 presents a comparative analysis of key actuation parameters for different types of TFAs, including bending curvature, response rate, actuation force, power density, and work capacity. Each type of actuation mechanism exhibits inherent advantages and trade-offs between its performances. TFAs driven by thermal stimuli (TdTFAs) usually demonstrate large output force (~200 mN)[86] and high durability (>10^7 cycles)[87]. However, their long response time (on the order of minutes) and hysteresis result in low power density and poor control accuracy, making them unsuitable for applications requiring rapid response and high-frequency motion, like bionic wings. In contrast, electro-driven TFAs (EdTFAs) exhibit rapid response (0.1 ~ 1 s) and high-frequency operation capability (e.g., 10 Hz for IP-based TFAs and 50 ~ 500 Hz for DE-based TFAs)[88]. Their motion can be precisely controlled via electrical signal modulation, making them well-suited for soft robotics and flexible electronics. However, these TFAs rely on external power sources and exhibit limited durability (~5000 cycles)[89] due to material aging under prolonged voltage application. Additionally, their output force will drop at high frequencies due to dielectric losses (~50% reduction at 100 Hz)[90]. Although light-driven TFAs (LdTFAs) show moderate actuation performance, their unique advantages of remote controllability and spatial selectivity (μm-level precision)[91] are invaluable for confined space exploration and minimally invasive surgery. Humidity-/Chemical-driven TFAs (HdTFAs/CdTFAs) always generate large deformations (~4 cm^{-1})[92], but show long response time (10 ~ 60 s) and limited output force (1 ~ 10 mN)[78], restricting their use in applications requiring high work capacity. Nevertheless, environmental signal responsiveness offers them distinct benefits for applications like wearable devices, sensors, and targeted drug release. These comparisons reveal that the choice of actuation mechanism should strike a careful balance between performance capabilities and application-specific

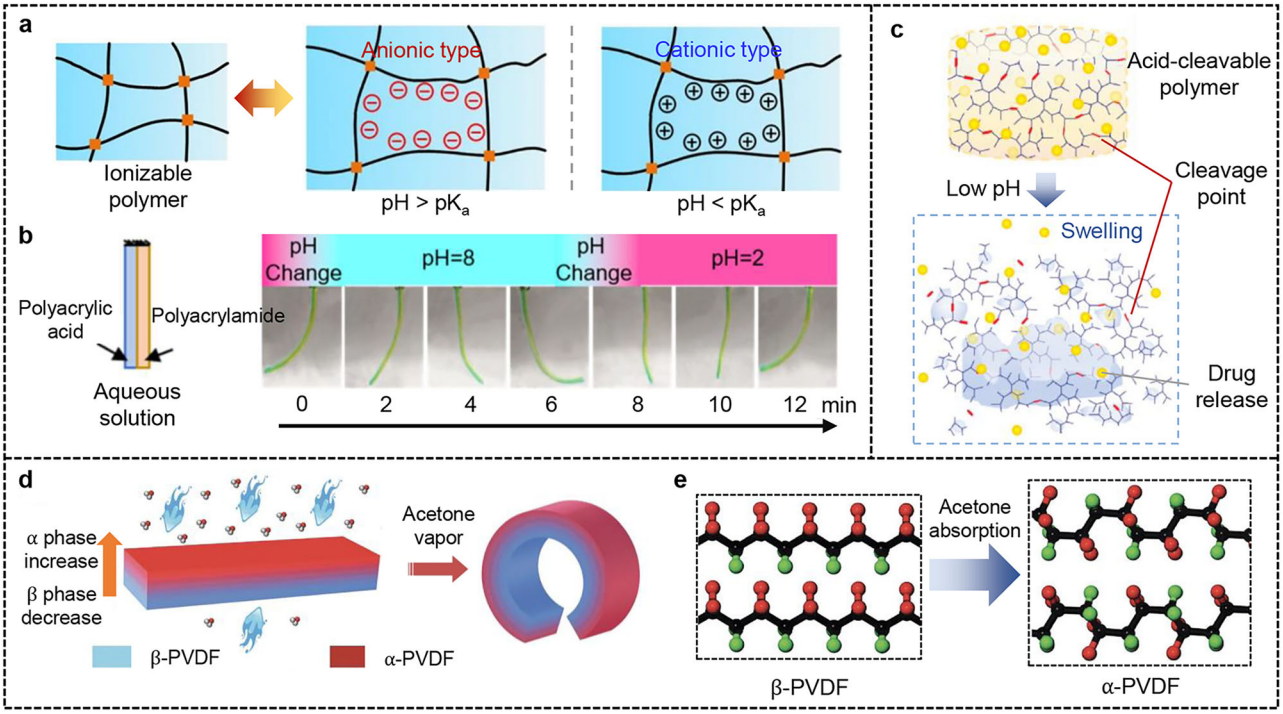

Fig. 8 | Typical CdTFAs. a Deformation mechanism of ionizable polymers. **b** Bidirectional bending of polyacrylamide/polyacrylic acid CdTFAs in different pH solutions. **c** Deformation mechanism of polymers containing acid-cleavable groups. **d** Deformation mechanism of organic-solvent-responsive PVDF-based CdTFAs. **e** Molecular structure of α-PVDF and β-PVDF. **a** Reprinted with permission from ref. 120. Copyright 2019 Springer Nature. **b** Reprinted with permission from ref. 47. Copyright 2020 American Chemical Society. **c** Reprinted with permission from ref. 84. Copyright 2023 MDPI. **d**, **e** Reprinted with permission from ref. 48. Copyright 2017 Royal Society of Chemistry.

demands. Development of TFAs with more balanced performance profiles can be achieved by material selection and structural optimization. However, many reviews have summarized these outcomes[19,93,94], so we will not delve into a detailed discussion on these aspects herein.

Applications Of TFAs

The deformation mechanisms of various TFAs provide insights into how external stimuli trigger the mechanical motion of TFAs. For their lightweight, high flexibility, high sensitivity, and programmability, TFAs hold tremendous promise in various applications, especially in biomimetic soft robotics, energy harvesting systems, and smart wearable devices.

Biomimetic soft robotics

TFAs possess low rigidity and are responsive to a variety of stimuli, making them quite suitable for applications in biomimetic soft robotics. They have been used to replicate plant morphing behaviors, such as blooming of narcissus flowers[22] (Fig. 10a), petal curling and bud opening of lotus and peony[95] (Fig. 10b), and the light-induced opening of water lily[45] (Fig. 10c). Additionally, TFAs can be applied to simulate flying creatures, including the magnet-driven biomimetic buttlefly[96] (Fig. 10d) and electro-driven biomimetic dragonfly[97] (Fig. 10e).

Beyond simple morphological imitation, TFAs enable the locomotion of functional robotics inspired by natural species. For instance, the crawling motion of worms was duplicated via TFAs. One approach to achieve directional crawling is to generate and apply direction-dependent friction on the actuator[98] (Fig. 10f). An alternative way to achieve directional locomotion is to leverage substrates with rachet-like structures[99] (Fig. 10g). Animal motions with more degrees of freedom, such as the serpentine locomotion of snakes[100] (Fig. 10h) and crawling of crabs[101] (Fig. 10i), were successfully emulated using TFAs. Beyond locomotion, TFAs have also been used to produce biomimetic claw[26] (Fig. 10j) and hand[102] (Fig. 10k) to realize grabbing function.

Energy harvesting systems

TFAs can convert external stimuli into electrical energy through various mechanisms. A direct approach is to apply the principle of electromagnetic induction to convert the dynamic energy of TFAs into electrical energy. For example, a HdTFA placed in a magnetic field generates electricity under the stimulation of humid airflow[103] (Fig. 11a, b). Another approach for generating electricity with TFAs leverages the piezoelectric effect, which generates electricity through promoted directional proton diffusion under pressure. For example, a HdTFA was developed by using MXene, cellulose, and a piezoelectric material made of polystyrene sulfonic acid (PSSA). Under humidity stimulation, the generator produces electricity with a high power density of 81.2 μW/cm³ and an open-circuit voltage of 0.3 V[104] (Fig. 11c, d). Additionally, TFAs can also generate electricity through the triboelectric effect, where frictional contact between positive and negative layers induces electrical charge. In such TFAs, frictional contact is usually achieved by sandwiching the friction layers between the inert and active layers. For instance, a TdTFA was developed by using LCE as the active layer and a conductive tape as the inert layer, while laminating the PVDF (negative friction layer) and nylon 6/6 (positive friction layer) inside. When temperature increases, this TdTFA will bend and generate open-circuit voltage of 2.1V[105] (Fig. 11e, f). Moreover, ion migration has also been applied in energy harvesting systems driven by TFAs. For example, the bending deformation of a HdTFA promotes the directional sodium ion migration within Poly(sodium 4-styrenesulfonate) (PSS), yielding a current of 32 μA[106] (Fig. 11g, h).

Smart wearable devices

The inherent flexibility and programmability of TFAs make them extensively useful in diverse wearable devices[107]. Exciting applications include smart textiles, human-machine interaction, and healthcare devices.

Integration with HdTFAs or TdTFAs endowed textiles with the ability to autonomously respond to sweat and heat generated by skin, enabling

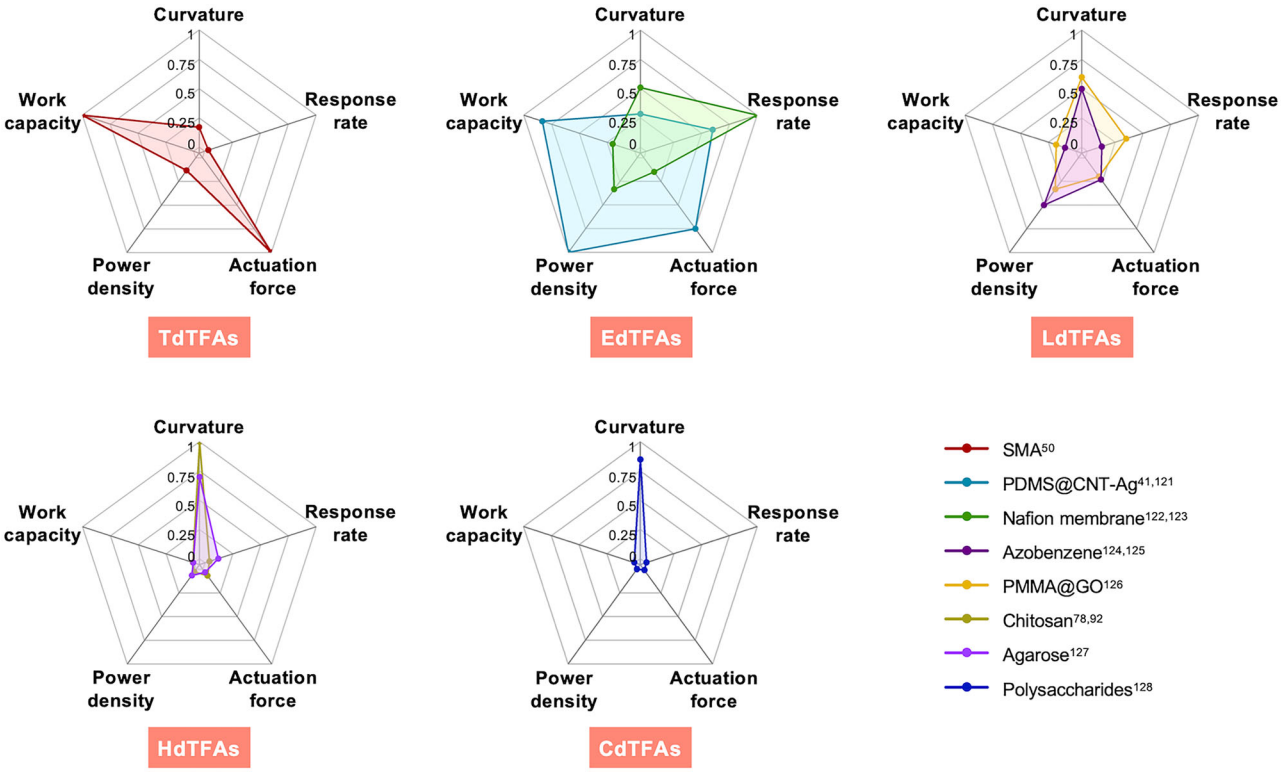

Fig. 9 | Radar charts comparing the performance of representative TFAs in five aspects including bending curvature, response rate, actuation force, power density, and work capacity. All data are normalized by the highest value among the selected TFAs: max. curvature: 4 cm^{-1}, max. response rate: 3 $cm^{-1} \cdot s^{-1}$, max. actuation force: 200 mN, max. power density: 15 W/kg, and max. work capacity: 600 J/kg. Selected TFAs include SMA-based TdTFAs[50], PDMS-based EdTFAs[41,121], Nafion-based EdTFAs[122,123], Azobenzene-based LdTFAs[124,125], PMMA-based LdTFAs[126], Chitosan-based HdTFAs[78,92], Agarose-based HdTFAs[127], and polysaccharide-based CdTFAs[128].

dynamic humidity and thermal management for enhanced wearer comfort. One representative design is the ventilating holes of smart sportswear. Figure 12a shows the prototype of smart sportswear with an array of microorganism/latex winglets[108]. When skin humidity increases, hygroscopic swelling of the microorganism layer triggers the winglets to open, creating breathable pores on the clothing. The increased airflow will dissipate heat and reduce perspiration. Another example applied HdTFA to modulate the thickness of fabrics[109]. When humidity increases due to sweating, the different swelling between the top and bottom sides of the arched HdTFAs causes them to flatten (Fig. 12b), resulting in reduced inter-fabric gaps and lower thermal insulation.

In addition to extending wearers' ability to adapt to the environment, TFAs, as wearable haptic devices, can also augment wearers' physiological functions, which is particularly valuable for handicapped people. Figure 12c shows a wearable haptic device equipped with a dielectric elastomer-based EdTFA[110]. The TFA gently compresses the skin at the rest state. When electrified, it undergoes an in-plane expansion, stretching the skin and generating different tactile feedback within a frequency range of 1 to 500 Hz. These haptic devices are incorporated with photodiode sensors, which function as a switch to detect the color on the paper (Fig. 12d). These devices can act as "haptic displays", enabling blind users to identify letters.

When integrated with thin-film sensors, TFAs can be applied as a wearable health monitoring device for real-time physiological assessment. For instance, Ling *et al.* integrated an electrothermal PI/PDMS-based TFAs with electrophysiological sensors[111] (Fig. 12e). This integrated system operates through a closed-loop feedback cycle, enabling autonomous wrapping around human fingers for reciprocating electrocardiogram (ECG) measurements. Joule heating induces TFA bending to wrap around a finger, initiating ECG measurement. When an ECG signal is detected, the electrical heating is deactivated, allowing TFA to revert. When the sensor loses contact with the finger, heating reactivates to restore contact and resume monitoring[112] (Fig. 12f).

Conclusion And Outlook

In this review, we comprehensively overviewed the research progress of TFAs with a focus on basic structures and mechanics, concerned responsive materials, deformation mechanisms, and applications. On the whole, each type of TFAs has its unique pros and cons. For a better selection of proper TFAs, the advantages and disadvantages of different types of TFAs are compared in Table 2. In particular, TFAs driven by light, thermal, and humidity stimuli can respond to environmental changes without any external power supply, and the autonomous and cyclic responses under steady stimulation indicate their significant potential for energy harvesting in Internet of Things (IoT) and environment monitoring. Additionally, the superior controllability of EdTFAs enables precise motion control in biomimetic soft robotics. Their precise controllability and high programmability make them ideal for biomimetic robotics requiring complex, multidimensional deformation. Moreover, their flexibility and durability position them as key components in wearable devices for human health monitoring and human-machine interaction. Despite these achievements and progress, TFAs are still at their early stage of development, necessitating continuous efforts for further advancement especially in the following aspects:

Performance enhancement

TFAs show great application potential in nanogenerators and biomimetic robotics, yet their performance remains unsatisfactory for real-life applications. For example, TFA-based nanogenerators exhibit lower energy transfer efficiency and power output, making them unsuitable for practical energy generators. Beyond energy, the force generated by TFAs is limited, while the application in soft robotics including grippers requires the TFAs to

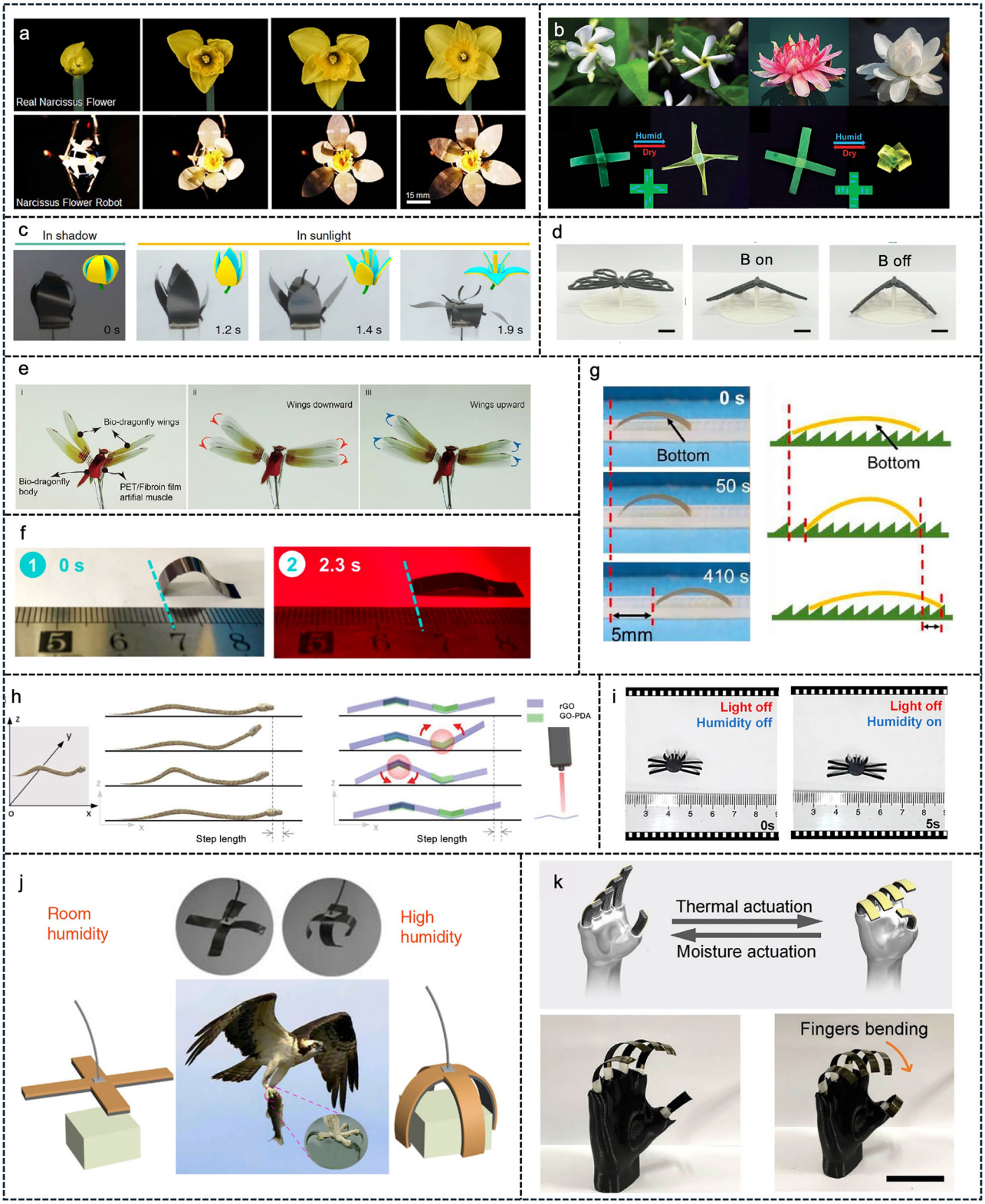

Fig. 10 | Applications of TFAs in biomimetic soft robotics. **a** Light-driven biomimetic narcissus flower. **b** Humidity-driven artificial lotus and peony. **c** Thermo-driven artificial water lily. **d** Magnet-driven biomimetic butterfly. **e** Electro-driven biomimetic dragonfly. **f** Light-driven crawling soft robotic. **g** Thermo-driven crawling soft robotic. **h** Light-driven biomimetic snake. **i** Humidity-driven biomimetic crab. **j** Humidity-driven biomimetic hawk claw. **k** Thermo-driven biomimetic human hand. **a** Reprinted with permission from ref. 22. Copyright 2019 American Association for the Advancement of Science. **b** Reprinted with permission from ref. 95. Copyright 2021 Wiley-VCH. **c** Reprinted with permission from ref. 45. Copyright 2020 Springer Nature. **d** Reprinted with permission from ref. 96. Copyright 2021 American Chemical Society. **e** Reprinted with permission from ref. 97. Copyright 2024 Wiley-VCH. **f** Reprinted with permission from ref. 98. Copyright 2021 American Chemical Society. **g** Reprinted with permission from ref. 99. Copyright 2023 Elsevier. **h** Reprinted with permission from ref. 100. Copyright 2019 Wiley-VCH. **i** Reprinted with permission from ref. 101. Copyright 2024 American Chemical Society. **j** Reprinted with permission from ref. 26. Copyright 2019 Springer Nature. **k** Reprinted with permission from ref. 102. Copyright 2023 Wiley-VCH.

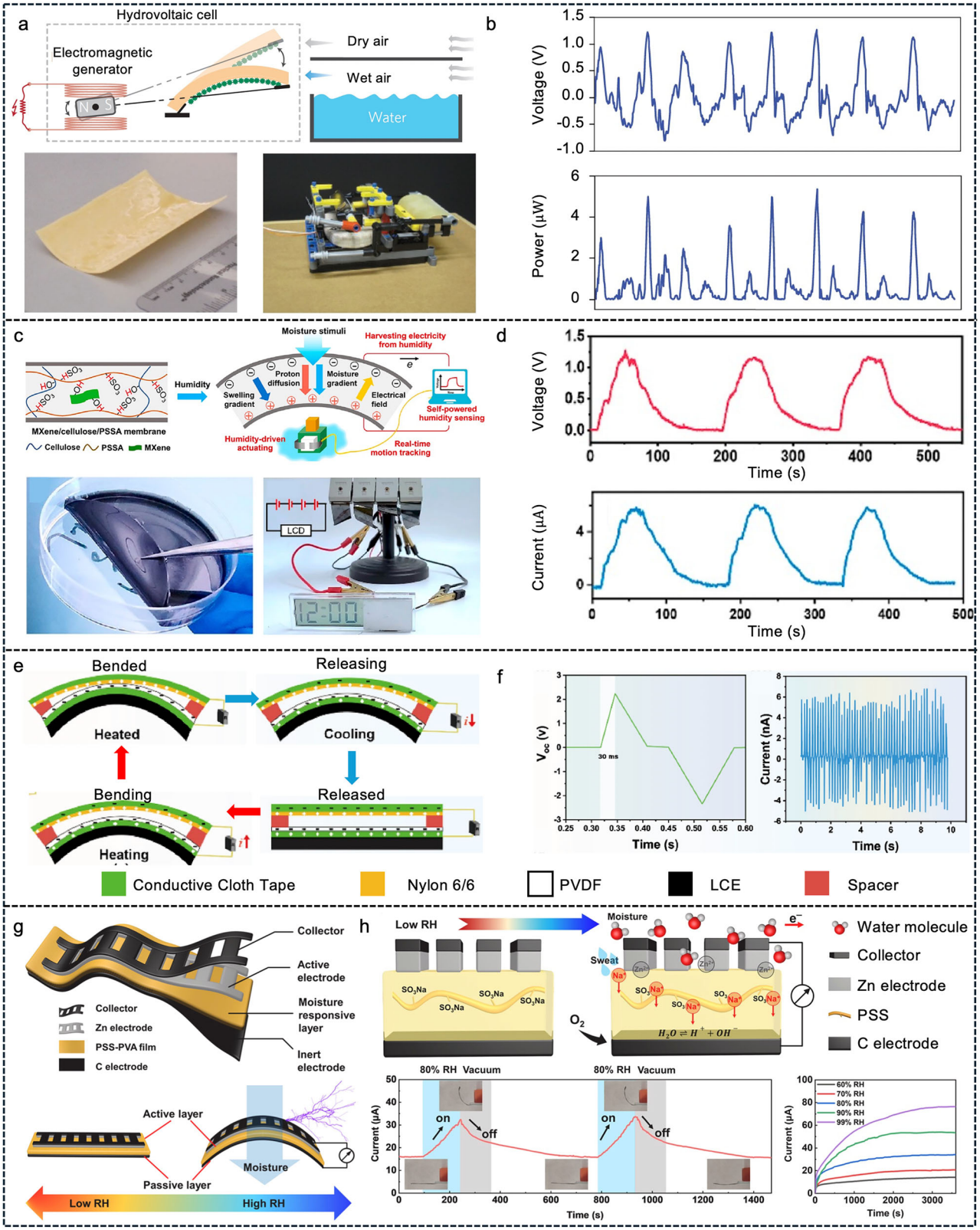

Fig. 11 | Applications of TFAs in energy harvesting systems. **a** HdTFAs-based nanogenerator. **b** Voltage and power output of the hydrovolcanic cell. **c** MXene/Cellulose/PSSA film-based nanogenerator. **d** Voltage and current output of the nanogenerator. **e** Working principle of HdTFAs-based triboelectric generator. **f** Voltage and current output of the HdTFAs-based triboelectric generator. **g** Snapshots of HdTFA-based generator. **h** Working principles and current output of the HdTFA-based generator. **a, b** Reprinted with permission from ref. 103. Copyright 2014 Springer Nature. **c, d** Reprinted with permission from ref. 104. Copyright 2021 American Chemical Society. **e, f** Reprinted with permission from ref. 105. Copyright 2023 Elsevier. **g, h** Reprinted with permission from ref. 106. Copyright 2024 Elsevier.

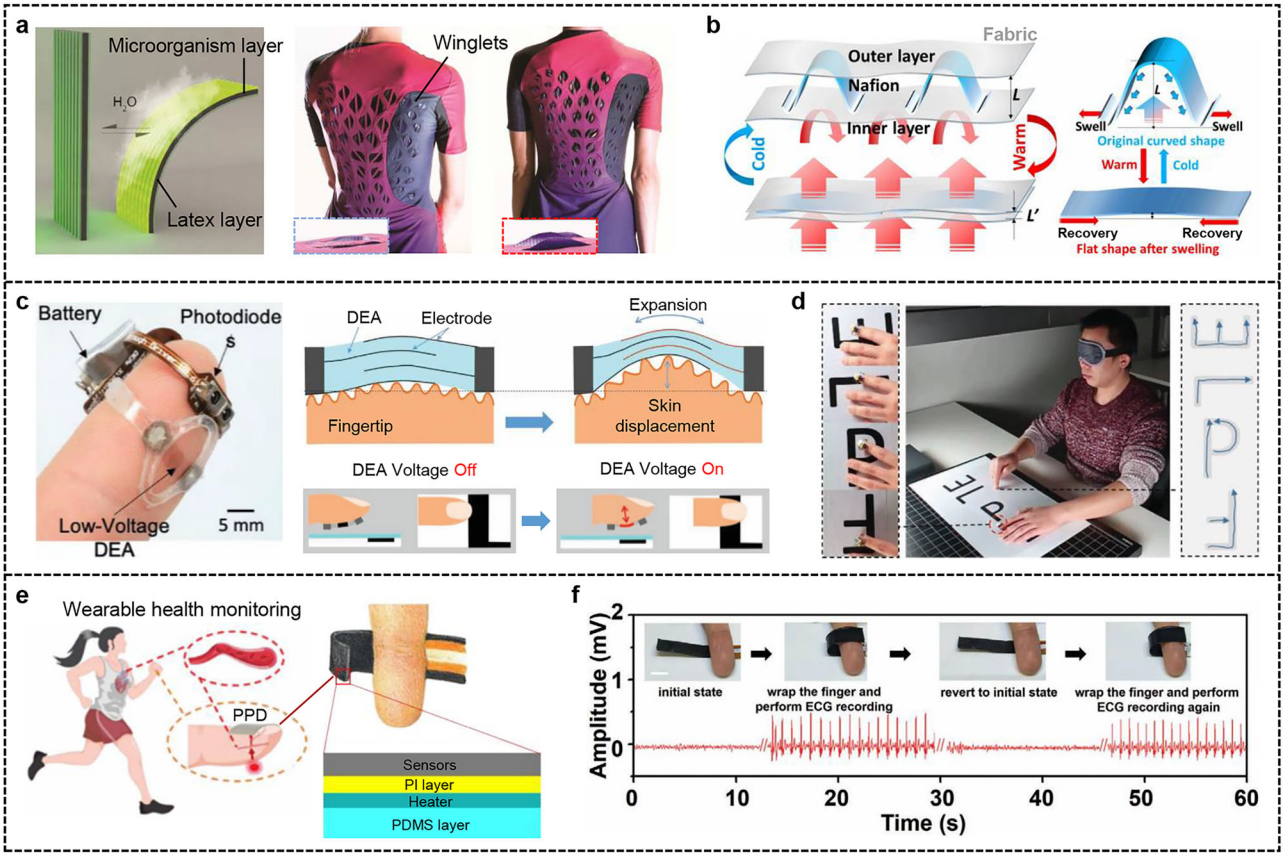

Fig. 12 | Applications of TFAs in smart wearable devices. a Sportswear prototype with microorganism/latex winglets. **b** A thickness-adjustable textile achieved by Nafion HdTFAs and their working principle. **c** Haptic device on a fingertip integrated with electronics and rechargeable battery and their working principle. **d** The blindfolded user correctly identifies all letters. **e** A wearable device for electrocardiogram monitoring. **f** Reciprocating electrocardiogram measurements by TFAs integrated with electrophysiological sensors. **a** Reprinted with permission from ref. 108. Copyright 2017 American Association for the Advancement of Science. **b** Reprinted with permission from ref. 109. Copyright 2017 Springer Nature. **c**, **d** Reprinted with permission from ref. 110. Copyright 2021 Wiley-VCH. **e**, **f** Reprinted with permission from ref. 112. Copyright 2020 Wiley-VCH.

Table 2 | Comparison of features among different types of TFAs

	TFA type				
Features	**Thermo-driven**	**Electro-driven**	**Light-driven**	**Humidity-driven**	**Chemical-driven**
Fast response	✗	✓	✗	✗	✗
Precisely controllable	✗	✓	✓	✗	✗
High sensitivity	✓	✓	✗	✗	✓
Wirelessly controllable	✓	✗	✓	✓	✗
Energy-efficient	✗	✓	✓	✓	✓
Scalable production	✓	✓	✓	✗	✓
Degradation of responsive materials	✓	✗	✓	✓	✓

exert controllable force to lift objects of varying shapes, weight, and fragility. Addressing these challenges requires an in-depth understanding of the mechanics governing actuation, including comprehensive studies to quantify how material properties influence performance and the development of scaling law for different actuations to enable on-demand customization. Moreover, the response speed of TFAs is low. For HdTFAs and TdTFAs, the signal transmission through air is slow and susceptible to environmental fluctuations. To address this problem, encapsulation and environmental isolation are applied to restrict the exposure to uncontrolled signals and hence to improve signal fidelity. For LdTFAs, it requires additional time to convert light energy into heat and subsequently into mechanical deformation, leading to significant energy losses. The current solution focuses on increasing the photothermal transition efficiency, by changing the microstructure of active materials to increase their light-exposed surface area, or doping other materials with high photothermal conversion efficiency (GO, CNT, etc.) in the active layer, or applying organic photothermal dyes or polymer materials with high photothermal efficiency. As actuator size increases, these limitations become more prominent due to the higher stimulation power required for large-scale operation, and the methods to improve energy efficiency become more important.

Improvement of durability and lifespan

Many materials used in TFAs suffer from low sustainability and durability. For example, elastomers and polymers, commonly used in EdTFAs and

LdTFAs, degrade under prolonged exposure to light and high temperatures. Solutions to such problems include introducing thermal stabilizers that can interrupt the degradation chain reaction of elastomers, crosslinking and vulcanization with other elements (e.g., sulfur vulcanization) to prevent thermal degradation, and adding inorganic fillers (e.g., TiO_2, ZnO) to absorb oxidation radiation. On the other hand, HdTFAs and CdTFAs tend to undergo structural deterioration due to reactions with water molecules or chemical reactants. For example, MXene is prone to be oxidized in moisture, which greatly limits the lifespan of the related hygroscopic actuators. To address these issues, proper preservative methods should be taken to preserve its chemical stability without sacrificing the hygroscopicity and mechanical properties. Therefore, conventional processes like surface passivation and encapsulation are not suitable for MXene-based HdTFAs, and novel methods including a modified mild synthesis process and adding antioxidants post-etching during synthesis are recommended.

Scalable manufacturing

Most of the current TFAs are produced on a small scale. For materials like SMAs, elastomers, and polymers, the existing fabrication methods such as rolling, cutting, and molding enable mass production. However, these methods are ineffective for 2D materials (e.g., MXene and GO) and fiber materials including carbon nanofibers and electro-spun fibers, as these materials are usually fragile and prone to fracture or delamination upon mechanical stress. Traditional fabrication protocols, which involve high pressure and shear stress, can tear and crumple the structure of these materials. While advanced technologies such as spin coating, spray coating, vacuum filtration, and blade coating achieve low thickness and smooth surfaces of these materials, they remain limited to centimeter-scale samples. Recent advanced technologies, including PVD and CVD, large-scale blade coating, and electrospinning, enabled the deposition of 2D materials onto larger substrates, unlocking the potentials for mass production in engineering.

Multifunctionality

Most TFAs are only able to respond to a single stimulus. Multifunctional TFAs should have the capability to respond to multiple different stimuli. Current multifunctional TFAs are often composed of multiple layers of responsive materials, which reduces their flexibility. To address these challenges, advanced fabrication techniques such as inkjet printing and laser sintering have been explored. However, each method presents pros and cons. For example, inkjet printing enables the fabrication of complex and highly precise structures, but its scalability for mass production remains limited. In parallel, the discovery of new materials offers another promising avenue. Monolithic materials such as MXene and bacterial cellulose have shown responsiveness to multiple stimuli, including humidity, temperature, and light. Nevertheless, their application in multifunctional TFAs is still in its initial state, largely due to intrinsic trade-offs between desirable material properties and multi-responsiveness. For instance, water-induced swelling in MXene films significantly reduces their electrical conductivity and mechanical stiffness. Furthermore, the deformation mechanisms of multifunctional TFAs become increasingly complex when exposed to simultaneous and heterogeneous stimuli. Understanding and unifying these mechanisms is crucial, as it would allow for the accurate prediction and control of TFA behavior in real-world, dynamic environments.

System-level integration

Many practical applications—such as wearable devices, soft robotics, and artificial muscles—require TFAs to be integrated with sensing, power, and control systems. Such system-level integration opens a door to numerous opportunities, especially through the incorporation of artificial intelligence (AI). AI-driven methods such as deep learning and model predictive control can enable TFAs to adapt to dynamic and complex environments. Moreover, AI can be employed to optimize material compositions and structural designs, enhancing TFA performance. For instance, EdTFAs-based sensors have achieved 88.6% object recognition accuracy using only strain and frequency data, enabled by embedded machine learning algorithms[113]. Similarly, AI-assisted path planning improved the motion efficiency of a centipede-inspired soft robot by 33%[114]. With continued advancements, TFAs could achieve near-perfect accuracy and efficiency. However, several challenges remain. First, transmitting data from TFAs to processing units typically involves wireless modules such as Bluetooth or NFC, which increases electrical integration complexity. Second, achieving high sensing accuracy often requires attaching flexible circuits or advanced receptors to TFAs, which can compromise the system's overall flexibility and durability. Additionally, interfacing TFAs with power supplies and control systems is difficult. For example, embedding sensors within nanoflake stacks to enable closed-loop control presents significant fabrication challenges. To address these issues, advanced manufacturing techniques—including multi-material 3D printing, soft lithography, and bioengineering—are being explored. Although research on the system-level integration of TFAs is still in its early stages, its promising potential is expected to drive forward the fields of materials science, soft robotics, and intelligent systems.

To fully unlock the potential of TFAs, future research efforts should be made with a focus on the enhancement of performance, improvement of durability, development of scalable manufacturing processes, and integration of multiple functions. Addressing the bottleneck technical problems in these aspects will facilitate the transition of TFAs from laboratory prototypes to real-life products and make them exceptionally applicable in next-generation soft robotics, biomedical devices, and Internet of Things.

Data Availability

No datasets were generated or analysed during the current study.

Received: 30 March 2025; Accepted: 18 June 2025;
Published online: 01 August 2025

References

1. Janocha, H. *Actuators*. (Springer, 2004).
2. Okuzaki, H. *Soft Actuators*. 2 edn, (Springer, 2019).
3. Runciman, M., Darzi, A. & Mylonas, G. P. Soft robotics in minimally invasive surgery. *Soft Rob* **6**, 423–443 (2019).
4. Li, H., Bai, H., Wang, Z., Tan, Y. & Tang, Y. Soft bioinspired pneumatic actuator for adaptive grasping based on direct ink writing method. *Sens. Actuators, A* **367**, 115041 (2024).
5. Pancaldi, L., et al. Flow driven robotic navigation of microengineered endovascular probes. *Nat. Commun.* **11**, 6356 (2020).
6. Hines, L., Petersen, K., Lum, G. Z. & Sitti, M. Soft actuators for small-scale robotics. *Adv. Mater.* **29**, 1603483 (2017).
7. Baughman, R. H. et al. Carbon nanotube actuators. *Science* **284**, 1340–1344 (1999).
8. Zhu, C., Lu, Y., Jiang, L. & Yu, Y. Liquid crystal soft actuators and robots toward mixed reality. *Adv. Funct. Mater.* **31**, 2009835 (2021).
9. Kim, M. S., Lee, H. T. & Ahn, S. H. Laser controlled 65 micrometer long microrobot made of Ni-Ti shape memory alloy. *Adv. Mater. Technol.* **4**, 1900583 (2019).
10. Kim, J., Hanna, J. A., Byun, M., Santangelo, C. D. & Hayward, R. C. Designing responsive buckled surfaces by halftone gel lithography. *Science* **335**, 1201–1205 (2012).
11. Cangialosi, A. et al. DNA sequence–directed shape change of photopatterned hydrogels via high-degree swelling. *Science* **357**, 1126–1130 (2017).
12. Ji, Z. et al. Morphable three-dimensional electronic mesofliers capable of on-demand unfolding. *Sci. China Mater.* **65**, 2309–2318 (2022).
13. Lee, H.-T., Lee, K.-I., Jang, K.-H. & Ahn, S.-H. Shape memory alloy-based microscale bending actuator fabricated by a focused ion beam chemical vapor deposition (FIB-CVD) gap-filling process. *Int. J. Precis. Eng. Manuf.* **21**, 491–498 (2020).
14. Breger, J. C. et al. Self-folding thermo-magnetically responsive soft microgrippers. *ACS Appl. Mater. Interfaces* **7**, 3398–3405 (2015).

15. Wu, Z. L., et al. Three-dimensional shape transformations of hydrogel sheets induced by small-scale modulation of internal stresses. *Nat. Commun.* **4**, 1586 (2013).
16. Zhang, C. et al. A review on reprogrammable bistable structures. *Smart Mater. Struct.* **33**, 093001 (2024).
17. Shin, B. et al. Hygrobot: A self-locomotive ratcheted actuator powered by environmental humidity. *Sci. Rob.* **3**, eaar2629 (2018).
18. Fu, S., Wei, F., Yin, C., Yao, L. & Wang, Y. Biomimetic soft microswimmers: from actuation mechanisms to applications. *Biomed. Microdevices* **23**, 1–13 (2021).
19. Li, M., Pal, A., Aghakhani, A., Pena-Francesch, A. & Sitti, M. Soft actuators for real-world applications. *Nat. Rev. Mater.* **7**, 235–249 (2022).
20. Ge, F., Lu, X., Xiang, J., Tong, X. & Zhao, Y. An optical actuator based on gold-nanoparticle-containing temperature-memory semicrystalline polymers. *Angew. Chem. Int. Ed.* **56**, 6126–6130 (2017).
21. Xuan, J. et al. Organic-base-driven intercalation and delamination for the production of functionalized titanium carbide nanosheets with superior photothermal therapeutic performance. *Angew. Chem. Int. Ed.* **55**, 14569–14574 (2016).
22. Umrao, S. et al. MXene artificial muscles based on ionically cross-linked $Ti_3C_2T_x$ electrode for kinetic soft robotics. *Sci. Rob.* **4**, eaaw7797 (2019).
23. Zhang, L. et al. Water-evaporation-powered fast actuators with multimodal motion based on robust nacre-mimetic composite film. *ACS Appl. Mater. Interfaces* **11**, 12890–12897 (2019).
24. Han, D.-D. et al. Bioinspired graphene actuators prepared by unilateral UV irradiation of graphene oxide papers. *Adv. Funct. Mater.* **25**, 4548–4557 (2015).
25. Wang, J. et al. Highly conductive MXene film actuator based on moisture gradients. *Angew. Chem. Int. Ed.* **59**, 14029–14033 (2020).
26. Dong, Y., et al. Multi-stimuli-responsive programmable biomimetic actuator. *Nat. Commun.* **10**, 4087 (2019).
27. Freund, L. B. & Suresh, S. *Thin film materials: stress, defect formation and surface evolution*. (Cambridge university press, 2004).
28. Li, Q. & Jiao, Y. Ultrafast photothermal actuators with a large helical curvature based on ultrathin GO and biaxially oriented PE films. *ACS Appl. Mater. Interfaces* **14**, 55828–55838 (2022).
29. Qiu, Y. et al. An asymmetric graphene oxide film for developing moisture actuators. *Nanoscale* **10**, 14060–14066 (2018).
30. Sun, L. et al. Multi-stimuli-responsive weldable bilayer actuator with programmable patterns and 3D shapes. *Adv. Funct. Mater.* **34**, 2311398 (2024).
31. Ha, M. et al. Reconfigurable magnetic origami actuators with on-board sensing for guided assembly. *Adv. Mater.* **33**, 2008751 (2021).
32. Kongahage, D. & Foroughi, J. Actuator materials: Review on recent advances and future outlook for smart textiles. *Fibers* **7**, 21 (2019).
33. Jeong, Y. et al. Biomimetic, programmable, and part-by-part maneuverable single-body shape-morphing film. *Adv. Intell. Syst.* **5**, 2200293 (2023).
34. Wang, W. et al. Multistimulus responsive actuator with GO and carbon nanotube/PDMS bilayer structure for flexible and smart devices. *ACS Appl. Mater. Interfaces* **10**, 27215–27223 (2018).
35. Sang, W. et al. Electrothermal actuator on graphene bilayer film. *Macromol. Mater. Eng.* **302**, 1700239 (2017).
36. Dong, L. L. & Zhao, Y. Photothermally driven liquid crystal polymer actuators. *Mater. Chem. Front.* **2**, 1932–1943 (2018).
37. Cai, G., Ciou, J.-H., Liu, Y., Jiang, Y. & Lee, P. S. Leaf-inspired multiresponsive MXene-based actuator for programmable smart devices. *Sci. Adv.* **5**, eaaw7956 (2019).
38. Lin, J. et al. Mechanical motion and modulation of thermal-actuation properties in a robust organic molecular crystal actuator. *Adv. Funct. Mater.* **32**, 2203004 (2022).
39. Wiranata, A. et al. High-frequency, low-voltage oscillations of dielectric elastomer actuators. *Appl. Phys. Express* **15**, 6 (2022).
40. Peng, J. B. et al. Dielectric elastomer actuators with low driving voltages and high mechanical outputs enabled by a scalable ultra-thin film multilayering process. *Adv. Funct. Mater.* **34**, 9 (2024).
41. Ahn, J. et al. Heterogeneous conductance-based locally shape-morphable soft electrothermal actuator. *Adv. Mater. Technol.* **5**, 1900997 (2020).
42. Kim, J., Jeon, J. H., Kim, H. J., Lim, H. & Oh, I. K. Durable and water-floatable ionic polymer actuator with hydrophobic and asymmetrically laser-scribed reduced graphene oxide paper electrodes. *ACS Nano* **8**, 2986–2997 (2014).
43. Tang, Z. H., Gao, Z. W., Jia, S. H., Wang, F. & Wang, Y. L. Graphene-based polymer bilayers with superior light-driven properties for remote construction of 3D structures. *Adv. Sci.* **4**, 10 (2017).
44. He, C. et al. Main-chain azobenzene poly(ether ester) multiblock copolymers for strong and tough light-driven actuators. *ACS Appl. Mater. Interfaces* **16**, 56469–56480 (2024).
45. Wang, S., et al. Asymmetric elastoplasticity of stacked graphene assembly actualizes programmable untethered soft robotics. *Nat. Commun.* **11**, 4359 (2020).
46. Fennimore, A. M. et al. Rotational actuators based on carbon nanotubes. *Nature* **424**, 408–410 (2003).
47. Han, Z. L. et al. Dual pH-responsive hydrogel actuator for lipophilic drug delivery. *ACS Appl. Mater. Interfaces* **12**, 12010–12017 (2020).
48. Deng, H. et al. An instant responsive polymer driven by anisotropy of crystal phases. *Mater. Horiz.* **5**, 99–107 (2018).
49. Ma, J.-N. et al. Multiresponsive MXene actuators with asymmetric quantum-confined superfluidic structures. *Adv. Funct. Mater.* **34**, 2308317 (2024).
50. Huang, X. et al. Highly dynamic shape memory alloy actuator for fast moving soft robots. *Adv. Mater. Technol.* **4**, 1800540 (2019).
51. Ware, T. H., McConney, M. E., Wie, J. J., Tondiglia, V. P. & White, T. J. Voxelated liquid crystal elastomers. *Science* **347**, 982–984 (2015).
52. Li, D. F. et al. Bioinspired ultrathin piecewise controllable soft robots. *Adv. Mater. Technol.* **6**, 8 (2021).
53. Chang, L., Wang, D., Jiang, A. & Hu, Y. Soft actuators based on carbon nanomaterials. *ChemPlusChem* **87**, e202100437 (2022).
54. Zhang, Y.-L. et al. Electro-responsive actuators based on graphene. *The Innovation* **2**, 100168 (2021).
55. Nguyen, V. H. et al. Stimuli-responsive MXene-based actuators. *Adv. Funct. Mater.* **30**, 1909504 (2020).
56. Hajiesmaili, E. & Clarke, D. R. Dielectric elastomer actuators. *J. Appl. Phys.* **129**, 151102 (2021).
57. Brochu, P. & Pei, Q. Advances in dielectric elastomers for actuators and artificial muscles. *Macromol. Rapid Commun.* **31**, 10–36 (2010).
58. Michel, S., Zhang, X. Q., Wissler, M., Löwe, C. & Kovacs, G. A comparison between silicone and acrylic elastomers as dielectric materials in electroactive polymer actuators. *Polym. Int.* **59**, 391–399 (2010).
59. Li, Z. et al. Cell Nanomechanics based on dielectric elastomer actuator device. *Nano Micro Lett* **11**, 98 (2019).
60. Zhang, H. et al. Low-Voltage Driven Ionic Polymer-Metal Composite Actuators: Structures, Materials, and Applications. *Adv. Sci.* **10**, 2206135 (2023).
61. Ling, Y. et al. Electrochemical actuators with multicolor changes and multidirectional actuation. *Small* **18**, 10 (2022).
62. Schmidt-Rohr, K. & Chen, Q. Parallel cylindrical water nanochannels in Nafion fuel-cell membranes. *Nat. Mater.* **7**, 75–83 (2008).
63. Acerce, M., Akdoğan, E. K. & Chhowalla, M. Metallic molybdenum disulfide nanosheet-based electrochemical actuators. *Nature* **549**, 370–373 (2017).
64. Li, K. R. et al. Lattice-contraction triggered synchronous electrochromic actuator. *Nat. Commun.* **9**, 11 (2018).

65. Vélez-Cordero, J. R. & Hernandez-Cordero, J. Heat generation and conduction in PDMS-carbon nanoparticle membranes irradiated with optical fibers. *Int. J. Therm. Sci.* **96**, 12–22 (2015).
66. Zhan, L. et al. Dual-responsive MXene-functionalized wool yarn artificial muscles. *Adv. Sci.* **11**, 2402196 (2024).
67. Xu, J.-W., Yao, K. & Xu, Z.-K. Nanomaterials with a photothermal effect for antibacterial activities: an overview. *Nanoscale* **11**, 8680–8691 (2019).
68. Deng, R.-H. et al. Nanoparticles from cuttlefish ink inhibit tumor growth by synergizing immunotherapy and photothermal therapy. *ACS Nano* **13**, 8618–8629 (2019).
69. Yang, Y. & Shen, Y. Light-driven carbon-based soft materials: principle, robotization, and application. *Adv. Opt. Mater.* **9**, 2100035 (2021).
70. Pang, X., Lv, J. A., Zhu, C., Qin, L. & Yu, Y. Photodeformable azobenzene-containing liquid crystal polymers and soft actuators. *Adv. Mater* **31**, 1904224 (2019).
71. Francis, W., Dunne, A., Delaney, C., Florea, L. & Diamond, D. Spiropyran based hydrogels actuators: Walking in the light. *Sens. Actuators, B* **250**, 608–616 (2017).
72. Irie, M., Fukaminato, T., Matsuda, K. & Kobatake, S. Photochromism of diarylethene molecules and crystals: memories, switches, and actuators. *Chem. Rev.* **114**, 12174–12277 (2014).
73. Kitagawa, D. et al. Control of photomechanical crystal twisting by illumination direction. *J. Am. Chem. Soc.* **140**, 4208–4212 (2018).
74. Kuenstler, A. S. & Hayward, R. C. Light-induced shape morphing of thin films. *Curr. Opin. Colloid Interface Sci.* **40**, 70–86 (2019).
75. Lu, X. L., Guo, S. W., Tong, X., Xia, H. S. & Zhao, Y. Tunable photocontrolled motions using stored strain energy in malleable azobenzene liquid crystalline polymer actuators. *Adv. Mater.* **29**, 7 (2017).
76. Jiang, Z., Xu, M., Li, F. Y. & Yu, Y. L. Red-light-controllable liquid-crystal soft actuators via low-power excited upconversion based on triplet-triplet annihilation. *J. Am. Chem. Soc.* **135**, 16446–16453 (2013).
77. Wang, M. et al. Bio-inspired high sensitivity of moisture-mechanical GO films with period-gradient structures. *ACS Appl. Mater. Interfaces* **12**, 33104–33112 (2020).
78. Tang, G. et al. Moisture-driven actuators. *Adv. Funct. Mater.* **35**, 2412254 (2024).
79. Lee, S., Lee, M. & Lee, J. Highly sensitive humidity-responsive actuator comprising aligned electrospun fibers containing metal-organic framework nanoparticles. *Sens. Actuators, B* **332**, 129520 (2021).
80. Chen, Q. et al. Cellulose-reinforced programmable and stretch-healable actuators for smart packaging. *Adv. Funct. Mater.* **32**, 2208074 (2022).
81. López-Díaz, A., Vázquez, A. S. & Vázquez, E. Hydrogels in soft robotics: Past, present, and future. *ACS Nano* **18**, 20817–20826 (2024).
82. Koetting, M. C., Peters, J. T., Steichen, S. D. & Peppas, N. A. Stimulus-responsive hydrogels: Theory, modern advances, and applications. *Mater. Sci. Eng.: R: Rep.* **93**, 1–49 (2015).
83. Kocak, G., Tuncer, C. & Bütün, V. pH-responsive polymers. *Polym. Chem.* **8**, 144–176 (2017).
84. de Campos, B. A., da Silva, N. C. B., Moda, L. S., Vidinha, P. & Maia-Obi, L. P. pH-sensitive degradable oxalic acid crosslinked hyperbranched polyglycerol hydrogel for controlled drug release. *Polymers* **15**, 1795 (2023).
85. Wang, Z. et al. PolyCOFs: A new class of freestanding responsive covalent organic framework membranes with high mechanical performance. *ACS Cent. Sci.* **5**, 1352–1359 (2019).
86. Lalegani Dezaki, M., Bodaghi, M., Serjouei, A., Afazov, S. & Zolfagharian, A. Adaptive reversible composite-based shape memory alloy soft actuators. *Sens. Actuators, A* **345**, 113779 (2022).
87. Bechtold, C., Chluba, C., Zamponi, C., Quandt, E. & de Miranda, R. L. Fabrication and characterization of freestanding NiTi based thin film materials for shape memory micro-actuator applications. *Shape Mem. Superelasticity* **5**, 327–335 (2019).
88. Ahn, J. et al. A review of recent advances in electrically driven polymer-based flexible actuators: Smart materials, structures, and their applications. *Adv. Mater. Technol.* **7**, 2200041 (2022).
89. Zhao, J., Wang, S., Zhang, Z., Yang, D. & Shao, J. Preparation and characterisation of IPMC brakes modified with composite electrodes performance. *Adv. Mech. Eng.* **16**, 16878132241286019 (2024).
90. Tang, C. et al. A review on high-frequency dielectric elastomer actuators: Materials, dynamics, and applications. *Adv. Intell. Syst.* **6**, 2300047 (2024).
91. Ube, T., et al. Spatially selective actuation of liquid-crystalline polymer films through two-photon absorption processes. *Nat. Commun.* **15**, 9430 (2024).
92. Xu, H. et al. An ultra-large deformation bidirectional actuator based on a carbon nanotube/PDMS composite and a chitosan film. *J. Mater. Chem. B* **7**, 7558–7565 (2019).
93. Apsite, I., Salehi, S. & Ionov, L. Materials for smart soft actuator systems. *Chem. Rev.* **122**, 1349–1415 (2022).
94. Pan, M. et al. Soft actuators and robotic devices for rehabilitation and assistance. *Adv. Intell. Syst.* **4**, 2100140 (2022).
95. Lan, R. et al. Humidity-responsive liquid crystalline network actuator showing synergistic fluorescence color change enabled by aggregation induced emission luminogen. *Adv. Funct. Mater.* **31**, 2010578 (2021).
96. Cao, X. et al. 3D printing magnetic actuators for biomimetic applications. *ACS Appl. Mater. Interfaces* **13**, 30127–30136 (2021).
97. Xiao, J. et al. Reprogrammable multi-responsiveness of regenerated silk for versatile soft actuators. *Adv. Funct. Mater.* **34**, 2316301 (2024).
98. Luo, X.-J. et al. Multifunctional $Ti_3C_2T_x$ MXene/low-density polyethylene soft robots with programmable configuration for amphibious motions. *ACS Appl. Mater. Interfaces* **13**, 45833–45842 (2021).
99. Chen, Z. et al. Dried bonito flakes-inspired moisture-responsive actuator with a gradient structure for smart devices. *J. Mater. Sci. Technol.* **167**, 152–160 (2023).
100. Yang, Y., Zhang, M., Li, D. & Shen, Y. Graphene-based light-driven soft robot with snake-inspired concertina and serpentine locomotion. *Adv. Mater. Technol.* **4**, 1800366 (2019).
101. Ma, B. et al. Quantum-confined-superfluidics-enabled multiresponsive MXene-based actuators. *ACS Appl. Mater. Interfaces* **16**, 15215–15226 (2024).
102. Bai, L. et al. Hygrothermic wood actuated robotic hand. *Adv. Mater.* **35**, 2211437 (2023).
103. Chen, X., Mahadevan, L., Driks, A. & Sahin, O. Bacillus spores as building blocks for stimuli-responsive materials and nanogenerators. *Nat. Nanotechnol.* **9**, 137–141 (2014).
104. Li, P., Su, N., Wang, Z. & Qiu, J. A $Ti_3C_2T_x$ MXene-based energy-harvesting soft actuator with self-powered humidity sensing and real-Time motion tracking capability. *ACS Nano* **15**, 16811–16818 (2021).
105. Zhang, Z. & Yuan, W. Highly biomimetic triboelectric-generating soft actuator with a hollow bilayer structure for sensing, temperature-sensitive switching and high-temperature alarm. *Compos. Sci. Technol.* **242**, 110185 (2023).
106. Zhan, L., et al. Moisture-triggered hybrid soft actuator and electric generator for self-sensing wearables and adaptive human-environment interaction. *Nano Energy* **132**, 110410 (2024).
107. Han, C. et al. Recent advances in sensor–actuator hybrid soft systems: Core advantages, intelligent applications, and future perspectives. *Adv. Sci.* **10**, 2302775 (2023).

108. Wang, W., et al. Harnessing the hygroscopic and biofluorescent behaviors of genetically tractable microbial cells to design biohybrid wearables. *Sci. Adv.* **3**, e1601984 (2017).
109. Zhong, Y., et al. Reversible humidity sensitive clothing for personal thermoregulation. *Sci. Rep.* **7**, 44208 (2017).
110. Ji, X. et al. Untethered feel-through haptics using 18-μm thick dielectric elastomer actuators. *Adv. Funct. Mater.* **31**, 2006639 (2021).
111. Wang, B., Zhou, S., Jiang, S., Qin, S. & Gao, B. Personalized medical devices connect monitoring and assistance: Emerging wearable soft robotics. *Anal. Chem.* **95**, 8395–8410 (2023).
112. Ling, Y. et al. Laser-induced graphene for electrothermally controlled, mechanically guided, 3D assembly and human-soft actuators interaction. *Adv. Mater.* **32**, 1908475 (2020).
113. Kim, J., Park, H. I. & Cha, Y. Thin film object recognition system using a two-legged piezoelectric actuator-sensor pair with machine learning. *Sens. Actuators, A* **375**, 115498 (2024).
114. Qu, J. et al. Advanced flexible sensing technologies for soft robots. *Adv. Funct. Mater.* **34**, 2401311 (2024).
115. Wang, Z. B., Chen, Y. X., Ma, Y. & Wang, J. Bioinspired stimuli-responsive materials for soft actuators. *Biomimetics* **9**, 26 (2024).
116. Xiao, Y. Y., Jiang, Z. C., Hou, J. B. & Zhao, Y. Desynchronized liquid crystalline network actuators with deformation reversal capability. *Nat. Commun.* **12**, 10 (2021).
117. Yang, Z. X., An, Y., He, Y. L., Lian, X. D. & Wang, Y. P. A programmable actuator as synthetic earthworm. *Adv. Mater.* **35**, 9 (2023).
118. Lee, E., Kim, D., Kim, H. & Yoon, J. Photothermally driven fast responding photo-actuators fabricated with comb-type hydrogels and magnetite nanoparticles. *Sci. Rep.* **5**, 8 (2015).
119. Liu, L. et al. Thermal concentration on thermoelectric thin film for efficient solar energy harvesting. *Coatings* **12**, 630 (2022).
120. Shi, Q. et al. Bioactuators based on stimulus-responsive hydrogels and their emerging biomedical applications. *Npg Asia Mater* **11**, 21 (2019).
121. Du, F., Wang, S., Chen, Z. & Li, Q. Stimuli responsive actuators: Recent advances. *J. Mater. Chem. C* **12**, 8217–8242 (2024).
122. Yang, L., Dongsheng, Z., Xining, Z., Aifen, T. & Ding, Y. Surface roughening of Nafion membranes using different route planning for IPMCs. *Int. J. Smart Nano Mater.* **11**, 117–128 (2020).
123. Guo, D., et al. PEDOT coating enhanced electromechanical performances and prolonged stable working time of IPMC actuator. *Sens. Actuators, B* **305**, 127488 (2020).
124. Ma, S., Li, X., Huang, S., Hu, J. & Yu, H. A light-activated polymer composite enables on-demand photocontrolled motion: Transportation at the liquid/air interface. *Angew. Chem. Int. Ed.* **58**, 2655–2659 (2019).
125. Chen, Y. et al. Light-driven bimorph soft actuators: design, fabrication, and properties. *Mater. Horiz.* **8**, 728–757 (2021).
126. Han, B. et al. Plasmonic-assisted graphene oxide artificial muscles. *Adv. Mater.* **31**, 1806386 (2019).
127. Zhang, L., Liang, H., Jacob, J. & Naumov, P. Photogated humidity-driven motility. *Nat. Commun.* **6**, 7429 (2015).
128. Duan, J., Liang, X., Zhu, K., Guo, J. & Zhang, L. Bilayer hydrogel actuators with tight interfacial adhesion fully constructed from natural polysaccharides. *Soft Matter* **13**, 345–354 (2017).

Acknowledgements

This work is supported by the Guangdong Basic and Applied Basic Research Foundation (No. 2024A1515013080, No. 2025A1515012192).

Author contributions

H.Y. planned and conceptualized the paper, provided supervision, guidance, and funding, and led the preparation of the paper. Z.Z. and Z.L. conducted the literature survey, wrote the original draft and created the figures and tables. All authors read and edited the paper.

Competing interests

The authors declare no competing interests.

Additional information

Correspondence and requests for materials should be addressed to Haimin Yao.